Computational and Structural Biotechnology Journal 19 (2021) 2423–2446

COMPUTATIONAL AND STRUCTURAL BIOTECHNOLOGY JOURNAL

journal homepage: www.elsevier.com/locate/csbj

Computational modeling and bioinformatic analyses of functional mutations in drug target genes in *Mycobacterium tuberculosis*

Pooja Singh [a,1], Salma Jamal [a,1], Faraz Ahmed [a,2], Najumu Saqib [a,2], Seema Mehra [a,2], Waseem Ali [a,2], Deodutta Roy [b], Nasreen Z. Ehtesham [c,*], Seyed E. Hasnain [d,e,*]

[a] *Jamia Hamdard Institute of Molecular Medicine, Jamia Hamdard, New Delhi 110062, India*
[b] *Department of Environmental and Occupational Health, Florida International University, Miami 33029, USA*
[c] *ICMR-National Institute of Pathology, Safdarjung Hospital Campus, New Delhi, India*
[d] *Department of Life Sciences, School of Basic Sciences and Research, Sharda University, Greater Noida 201301, India*
[e] *Department of Biochemical Engineering and Biotechnology, Indian Institute of Technology, Delhi (IIT-D), Hauz Khas, New Delhi 110016, India*

ARTICLE INFO

Article history:
Received 13 January 2021
Received in revised form 9 April 2021
Accepted 15 April 2021
Available online 19 April 2021

Keywords:
Tuberculosis
Genome sequencing
MDR
MycoTRAP-DB
Secondary mutations
SNPs

ABSTRACT

Tuberculosis (TB) continues to be the leading cause of deaths due to its persistent drug resistance and the consequent ineffectiveness of anti-TB treatment. Recent years witnessed huge amount of sequencing data, revealing mutations responsible for drug resistance. However, the lack of an up-to-date repository remains a barrier towards utilization of these data and identifying major mutations-associated with resistance. Amongst all mutations, non-synonymous mutations alter the amino acid sequence of a protein and have a much greater effect on pathogenicity. Hence, this type of gene mutation is of prime interest of the present study. The purpose of this study is to develop an updated database comprising almost all reported substitutions within the *Mycobacterium tuberculosis* (*M.tb*) drug target genes *rpoB*, *inhA*, *katG*, *pncA*, *gyrA* and *gyrB*. Various bioinformatics prediction tools were used to assess the structural and biophysical impacts of the resistance causing non-synonymous single nucleotide polymorphisms (nsSNPs) at the molecular level. This was followed by evaluating the impact of these mutations on binding affinity of the drugs to target proteins. We have developed a comprehensive online resource named MycoTRAP-DB (*Mycobacterium tuberculosis* Resistance Associated Polymorphisms Database) that connects mutations in genes with their structural, functional and pathogenic implications on protein. This database is accessible at http://139.59.12.92. This integrated platform would enable comprehensive analysis and prioritization of SNPs for the development of improved diagnostics and antimycobacterial medications. Moreover, our study puts forward secondary mutations that can be important for prognostic assessments of drug-resistance mechanism and actionable anti-TB drugs.

1. Introduction

Tuberculosis (TB) has been a deadly disease since 3400BCE with huge social and economic impact worldwide [1]. According to the WHO Global Tuberculosis Report, an estimated 10 million people developed TB in 2019 [2]. Globally, TB is among the top ten causes of death, with multi-drug resistance posing additional challenge in managing this global epidemic [3]. In 2019, it took relatively 1.2 million lives in HIV-negative people and 208,000 deaths amongst HIV-positive people. *Mycobacterium tuberculosis* (*M.tb*) pathogen circumvents new strategies by which it can find ways to infect, survive, and disseminate against the barriers set by the host [4]. The evolution of the *M.tb* genome has been crucial in maintaining its virulence throughout the centuries as the pathogen undergoes reductive evolution and confines its essential functionality to the minimum possible number of genes [5]. The alterations within the genome composition have been a crucial strategy for the pathogen to overcome the stresses and challenges posed by the environment or the host.

The extensive use of antibiotics against *M.tb* has been posing a threat to the existence of this pathogen, and in response *M.tb* has been rigorously selecting the strains that could help the pathogen

* Corresponding authors at: Department of Life Sciences, School of Basic Sciences and Research, Sharda University, NOIDA, NCR, India (S.E. Hasnain).
E-mail addresses: nzehtesham@gmail.com (N.Z. Ehtesham), seh@dbeb.iitd.ac.in (S.E. Hasnain).
[1] These authors contributed equally.
[2] These authors contributed equally.

https://doi.org/10.1016/j.csbj.2021.04.034

to survive against the antibiotic exposures [6,7]. With time, the mutations accumulated within the *M.tb* genome and specifically in the proteins serving as drug targets, have caused the development of resistance against various first and second lines anti-TB drugs and further its self-transformation into pre-extensively drug resistant (pre-XDR), multidrug resistant (MDR) and extensively drug-resistant (XDR) [7,8]. Drug efflux pumps, with a specific genetic signature could be yet other mechanism for drug resistance [9]. Mutations at the active site of protein precisely affect the binding efficacy of the drug or may leave the protein deprived of its catalytic efficiency. Such mutations are well characterized due to their major role in drug resistance, however there are other mutations present outside the active region, also termed as secondary or accessory mutations which are indirectly responsible for causing resistance [8,10]. Secondary mutations or accessory mutations cause noticeable rearrangements into the protein structure leading to altered drug interaction and affecting the dynamics of the complex by altering the shape and flexibility of the binding pocket through a complex network of interactions within the structure, defined as "network hypothesis" [11]. These mutations also assist in compensating the fitness cost developed due to the after effects of drug resistance mutations, hence termed as compensatory mutations [12]. It is thus of utmost importance to explore secondary mutations present in the neglected and less focused genomic areas for complete understanding of the mechanism of resistance.

We are also witnessing enormous amounts of genome sequencing data that are being assessed broadly to identify the polymorphisms of relative clinical significance and improve the understanding of drug resistance in *M.tb* [11–14]. However, the corresponding information is scattered among the large pool of literature, which renders the researchers to be deprived of the critical information which might be used for identification of novel drug targets and development of anti-TB drugs. Over the years, several databases [15] namely GMTVD [16], TBDreaMDB [17], MUBII-TB-DB [18] have been developed to store and organize data, but they are devoid of the recent records owing to which the conclusions are bound to remain incomplete. Thus, an extensive search of recent literature to acquire all the reported mutations is critical for understanding the evolution of anti-TB drug resistance.

Drug resistance-associated genes *rpoB*, *inhA*, *katG*, *pncA*, *gyrA* and *gyrB* are known to confer resistance against rifampicin (RIF), isoniazid (INH), pyrazinamide (PZA) and fluoroquinolones (ciprofloxacin, CIF; moxifloxacin, MFX; levofloxacin, LFX; and ofloxacin, OFX), respectively [7]. The mutations in these genes are responsible for detrimental effects over the normal functionality of protein serving as a target, disrupting its binding with the drug and subsequently leading to antibiotic resistance [19]. Single nucleotide polymorphisms (SNPs) are the most recurrent genetic variations responsible for disturbing protein functionality and promoting drug resistance in *M.tb*. Although many of these are benign or neutral and do not contribute much to the phenotypic alteration many others, primarily the non-synonymous mutations, are deleterious which have severe consequences on function of the translated protein and its phenotype. Thus, it is imperative to look for the non-synonymous mutations reported in the drug-resistant isolates as they serve as key leads for explaining the mechanism of resistance development. Apart from SNPs, other variations that include insertions, deletions and frame-shift mutations are also major contributors towards drug resistance, however these were out of the scope of the present study and thus were not included.

In order to study the mechanisms of drug resistance, it is critically important to know the association between mutations in drug targets and their phenotypic profile by establishing minimum inhibitory concentrations (MICs). *In-vitro* propagation of *M.tb* is challenging because of its slow growing nature requiring time and resources. Alternative (*in-silico*) methods can help to prioritize mutations by predicting structural implications, due to the unavailability of a quantitative estimation of phenotypic profiling [20]. In the present study, a rigorous search of the recently reported literature on nearly all the mutations in well recognized drug resistance-associated genes *rpoB*, *inhA*, *katG*, *pncA*, *gyrA* and *gyrB* was performed [21]. Apart from these genes, *embC*, *embA*, and *embB* are also associated with resistance to ethambutol (EMB) [22] which is a first-line drug. However, in 2019, WHO released a new drug classification for the treatment of drug resistant TB, reorganizing second-line drugs into three groups (Group-A, B, and C). Ethambutol has been included in group C [23] and also serves as a key drug in second-line regimens for MDR-TB and thus was not included in this study. Various computational approaches were used to quantify the effects of non-synonymous substitutions over the protein structure, function, and conservation narrowing down our search for the candidates with higher potential of inducing the resistance. Further, molecular docking studies were carried out to examine the impact of the candidate mutations on drug-protein interaction eventually ending up with hampered drug efficacy. This was followed by normal mode analysis (NMA) performed to gain insights into the interaction profiles by taking into account the dynamic aspects of the protein which are requisite parameters for favorable protein-drug interaction, concluding our search for the potential novel active site and secondary mutations responsible for conferring the resistance [24]. The computational analyses and MycoTRAP-DB (*Mycobacterium tuberculosis* Resistance Associated Polymorphisms Database) platform serving as a high-throughput platform, could provide the scientific basis of an initiation to *in-vitro* studies that aim for an in-depth characterization of emerging potential resistance conferring mutations.

2. Methodology

Fig. 1 Illustrates all of the steps of computational methodology followed in the present study. These steps consist of: 1) Acquisition of publicly available data and construction of a library predictive of resistant and susceptible mutations in genes; 2) Determining SNPs as deleterious or neutral using PredictSNP tool; 3) Structural and thermodynamic change prediction showing the impact of mutations on protein stability and conformation using three tools based on different structural features; Site Directed Mutator (SDM), STRUM and mutation Cut-off Scanning Matrix (mCSM); 4) Determining the impact of mutations on protein-drug binding by molecular docking; 5) Identification of the dynamic interaction of mutation inflicted proteins. 6) Scoring conservation of WT and mutant residues; and 7) Protein-protein interaction network analysis. These steps are described in detail below:

2.1. Data acquisition and library preparation

A library predictive of resistant and susceptible mutations of *rpoB, inhA, katG, pncA, gyrA* and *gyrB* genes was prepared through a rigorous literature search. Mutations from the two publicly available databases, TBDreaMDB [17] and GMTVD [16] were also extracted. Furthermore, mutations reported by web-based tools, MUBII-TB-DB [18] and CRyPTIC Consortium [25] were also incorporated. Based on the intensive data mining of available literature, each SNP was represented as resistance causing, neutral or uncharacterized along with their frequency of occurrence in clinical isolates.

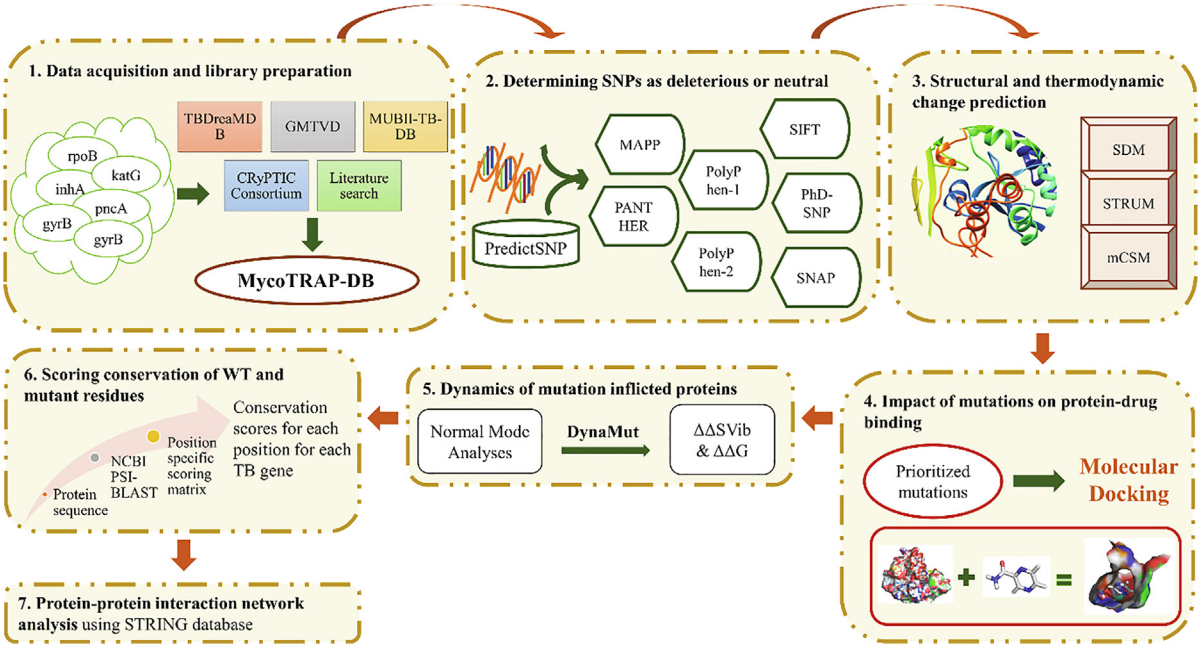

Fig. 1. Illustration of the workflow describing all of the steps of computational methodology consisting of: 1) Acquisition of publicly available data and construction of a library predictive of resistant and susceptible mutations in genes; 2) Determining SNPs as deleterious or neutral using PredictSNP tool; 3) Structural and thermodynamic change prediction showing the impact of mutations on protein stability and conformation using three tools based on different structural features; SDM, STRUM and mCSM; 4) Determining the impact of mutations on protein-drug binding by molecular docking; 5) Identification of the dynamic interaction of mutation inflicted proteins, 6) Scoring conservation of WT and mutant residues; and 7) Protein-protein interaction network analysis.

2.2. Determining SNPs as deleterious or neutral

The reference *M.tb* H_{37}Rv genome used was NC_000962.3. The protein sequences for the *M.tb* genes investigated in the present study were obtained from UniProt, which is a freely accessible database hosting protein sequence and functional data. The UniProt IDs for *rpoB, inhA, katG, pncA, gyrA* and *gyrB* corresponded to P9WGY9, P9WGR1, P9WIE5, I6XD65, P9WG47 and P9WG45. Characterization of non-synonymous (ns) SNPs as deleterious or neutral was performed using PredictSNP tool [26]. PredictSNP is a disease associated mutation classifier and gives a consensus score based on the output of six different amino acid (AA) based function and pathogenicity prediction tools, namely Multivariate Analysis of Protein Polymorphism (MAPP), nsSNPAnalyzer, Protein Analysis through Evolutionary Relationships (PANTHER), PhD-SNP, PolyPhen-1 and PolyPhen-2, Sorting Intolerant From Tolerant (SIFT), and Synonymous Non-synonymous Analysis Program (SNAP) (Table 1). MAPP calculates the difference in physicochemical properties between the wild and mutant AAs. Larger the deviation, higher is the chance that the mutation causes functional disruption of the protein. PANTHER is an evolutionary based tool which anticipates the function of hypothetical genes based on their evolutionary relationship to experimentally characterized genes with known function [27]. PhD-SNP is a support vector machine classifier-based method that predicts deleterious SNPs using sequence and profile information [28]. Polymorphism Phenotyping (PolyPhen) engages a set of empirical rules to determine the functional disruption in the presence of mutation [29]. PolyPhen-2 is different from PolyPhen-1 in terms of features used for prediction and uses eight sequence based and three structure-based AA properties for predicting the functional and structural damage due to AA substitutions [30]. SIFT is an evolutionary based algorithm which measures the impact of AA change on the function of protein based on physical properties and sequence homology [31]. SNAP is based on a set of codon-aligned nucleotide sequences which determine synonymous and non-synonymous substitution rates [32]. Consensus prediction made by PredictSNP represents an accurate and robust alternative to the predictions delivered by individual tools. The AA sequence of a query protein was uploaded in FASTA format on PredictSNP along with the list of mutations in a text format. PredictSNP web server gave consensus prediction along with the predictions made by the individual tools for all selected mutations.

2.3. Structural and thermodynamic change prediction

To examine the impact of mutations on protein stability and conformation, three tools based on different structural features; SDM, STRUM and mCSM were utilized. SDM calculates a stability score based on environment-specific AA substitution frequencies within homologous protein families [33]. The score is equivalent to the change in free energy (ΔΔG) between the wild-type (WT) and mutant protein. To further enhance the significance of SDM predictions, the nsSNPs that were submitted to SDM were also analyzed by STRUM which combines the WT protein sequence profiles with low-resolution structure models built by I-TASSER to calculate the fold stability change (ΔΔG) of protein molecules upon single-point mutations [34]. Lastly mCSM, a machine learning approach that integrates graph-based signatures, pharmacophore properties and experimental conditions and uses this information to calculate changes in the stability of protein structure [35] was used. The consensus ΔΔG score of all the three tools were considered to denote the impact of mutations on protein stability as highly destabilizing, destabilizing or stabilizing.

Based on the results drawn from various sequence and structure-based tools, consensus mutations, that were predicted to be functionally deleterious and structurally destabilizing, were derived and considered for further analyses.

Table 1
Computational tools used to study the impact of mutations on protein structure and function.

Software	Information	Description	Value/Range	PMID
MAPP	Physicochemical variation	Deleterious/ Neutral	–	15,965,030
PANTHER	Protein analysis through evolutionary relationship	Pathogenic/Deleterious	–	20,015,972
PolyPhen-1	Sequence, phylogenetic and structural information	Deleterious/ Neutral	–	12,202,775
PolyPhen-2	Eight sequence based and three structure based amino acid properties	Deleterious/ Neutral	0–1 ($\leq$0.15 tolerated, 0.15 $\leq$ 1.0 possibly damaging, 0.85 $\leq$ 1.0 damaging)	20,354,512
SIFT	Sequence homology and the physical properties of amino acids	Deleterious/ Neutral	0 ($\leq$0.05 pathogen; 0–1)	12,824,425
PhD-SNP	Support vector machine prediction trained on sequence and evolutionary information	Pathogenic/ Benign	0–1 ($\leq$0.5 benign, >0.5 pathogenic)	16,895,930
SNAP	Neural network method based on sequence information	Non-Neutral	reliability index measure (range 0–9)	17,526,529
SDM	Environment-specific substitution tables	Reduced stability/ Increased stability	$\Delta\Delta G < 0$ reduced stability; $\Delta\Delta G > 0$ increased stability	21593128, 28,525,590
STRUM	Sequence profile, structural profile, different energy functions based on I-TASSER model	Destabilizing/ stabilizing	$\Delta\Delta G < 0$ destabilizing; $\Delta\Delta G > 0$ stabilizing	27,318,206
mCSM	Graph-based signatures, pharmacophore properties and experimental conditions	Destabilizing/ stabilizing	$\Delta\Delta G < 0$ destabilizing; $\Delta\Delta G > 0$ stabilizing	24,281,696
mCSM-lig	Protein-ligand affinity change upon mutation	Destabilizing/ stabilizing	$\Delta\Delta G < 0$ destabilizing; $\Delta\Delta G > 0$ stabilizing	27,384,129

2.4. Impact of mutations on protein-drug binding

Molecular docking was performed to quantify the influence of mutations on the binding affinity of drugs targeting proteins encoded by *rpoB, inhA, katG, pncA, gyrA* and *gyrB* genes. An initial screening was done employing mCSM-lig. This is a freely available online tool that uses graph-based signatures of WT structural environment to assess the structural ramifications on drug binding due to mutations in the protein [36]. The mutations having strong destabilizing effects on protein-drug binding were subjected to docking using Schrodinger suite [37]. The X-ray crystal structures of WT proteins were obtained from Protein Data Bank (PDB) [38] and the structures represented by following PDB IDs: RpoB (5UHB) [39], InhA (1ENY) [40], KatG (1SJ2) [41] (recently a cryo-EM structure of katG was published [42] however it has not yet been released on PDB), PncA (3PL1) [43] and DNA gyrase (5BS8) [44]. The ligand bound crystal structures were available for RpoB, InhA and DNA gyrase (in complex with MFX). In case of mutations in InhA protein, ligand bound crystal structures were available only for I21V (PDB ID: 2AQH) [45] and S94A (PDB ID: 2NV6) [46]. The mutations in WT protein structures were incorporated by employing the Maestro interface available from Schrodinger. Prior to molecular docking, the WT and mutant protein structures were prepared using Schrodinger's protein preparation wizard [47]. Several tasks were performed during protein preparation which include deleting water molecules, repairing truncated sidechains, adding hydrogens and assigning partial charges. The chemical structures of the first line TB drugs (RIF, INH and PZA) and fluoroquinolones [48] were obtained from PubChem compound database [49] and were used as ligands in the present study. The ligands were prepared using the LigPrep module [47] which generated accurate and energy minimized conformations of compounds. The idea behind generating structurally diverse compounds is to explore all the chemical and structural properties a compound could possess as even small changes can amount to significant variations in computational results. Subsequent to this, a grid box was generated centered on the active site residues of the proteins using the Receptor Grid Generation module. The active site for each of the protein, RpoB, InhA, KatG, PncA and DNA gyrase, was acquired from literature [39,43,46,50,51]. Lastly, the ligands were docked in the active sites of WT and mutant proteins using the extra precision approach of Schrodinger's Glide module [52].

2.5. Dynamic interaction of mutation inflicted proteins

Proteins are highly dynamic in nature and their structural fluctuations have an important role in their functions. Therefore, it is quite imperative to assess the impact of mutations on the native conformations of proteins. Post molecular docking of the proteins were run on DynaMut, a web server that takes into account NMA and integrates it with graph-based structural signatures and gives a consensus prediction of the impact of a mutation on the stability of a protein [24]. NMA is a powerful technique for predicting molecular motions and examines the vibrational entropy changes due to harmonic oscillating fluctuations as a consequence of mutations in the protein [53]. Vibrational entropy changes ($\Delta\Delta S_{Vib}$ ENCoM in kcal.mol^{-1}.K^{-1}) and NMA predictions ($\Delta\Delta G$ ENCoM in kcal/mol) were recorded to examine the effect of mutations on protein flexibility and stability thus influencing overall protein dynamics.

2.6. Scoring conservation of WT and mutant residues

Conservation analysis of codons helps in understanding the evolutionary conservation of a particular residue in a protein that could be of structural and functional importance. Conservation scores are determined based on the AA frequencies at a certain codon in the alignment. To perform AA conservation analysis in the present study, the sequence for each protein, RpoB, InhA, KatG, PncA, GyrA and GyrB was downloaded from UniProt database [54] followed by a NCBI PSI-BLAST [55] run against the non-redundant protein database for each TB protein. A profile search was generated using five PSI-BLAST iterations with an e-value cut-off of 0.001. Next a position specific substitution matrix (PSSM) was generated, the elements of which were conservation scores for each position for each TB gene. The overall substitution score ranges from −8 to 10 where the positive value represents that the mutation is favorable, fit and evolution can accept this transition over normal WT codon during the time of need. On the other hand, negative values reflect the less likely mutations or mutations that result in altered functionality. For all nsSNPs, the conservation scores of all the substitutions were acquired. Additionally, a score for replacement of WT with mutant AA was analyzed which represents the substitution score. The mutations with high substitution score (>5 in this study) would be less detrimental for the overall

integrity of the protein and thus the normal function of the protein would not be hampered.

2.7. Protein-protein interaction network analysis

Protein-protein interaction (PPI) network was analyzed using STRING database version 11.0 for all TB proteins studied in this work. STRING (Search Tool for the Retrieval of Interacting Genes/Proteins) is a freely accessible web resource and biological database which harbors information about PPIs curated from numerous sources, including experimental data, computational prediction methods and public text literature collections [56].

3. Results and discussion

3.1. Data acquisition and library preparation

In the present study, we have assembled known mutations and present a database, MycoTRAP-DB for TB-protein coding genes, *rpoB*, *inhA*, *katG*, *pncA*, *gyrA* and *gyrB* from the previously published databases as well as thorough data mining of the available literature till December 2020. A repository comprising a total of 3303 mutations was prepared which included mutations from GMTVD, TBDreaMDB, MUBII-TB-DB and CRyPTIC Consortium. Moreover the remaining mutations, not included in the above databases, were acquired by rigorously searching the published literature related to the drug resistance in *M.tb* (Supplementary Table 1). The final collective mutations were 701, 56, 504, 476, 822, and 744 for *rpoB*, *inhA*, *katG*, *pncA*, *gyrA* and *gyrB* respectively. By removing the duplicates, synonymous mutations and point mutations leading to insertions and deletions, we obtained 1795 total mutations for further analysis. The final mutations obtained for *rpoB*, *inhA*, *katG*, *pncA*, *gyrA* and *gyrB* corresponded to a total of 406, 37, 446, 402, 258 and 246 mutations, which were further characterized based on their resistance conferring potential (Table 2).

3.2. Amino acid conservation and substitution analysis

Conservation score reflects the significance of a WT AA at a particular codon position in preserving the normal functionality of the protein [57]. On the other hand, the deviation from the normal function caused by a particular substitution based on newly inserted AA is depicted by substitution score. Analyzing these scores for all the AAs at a specific codon presented the information about evolutionarily favorable mutated AAs at that position. The conservation and substitution scores of all the AAs for each gene have been provided as Supplementary Table 2. The positive values for conservation scores showed the high degree of conservation of an AA at that position in retaining the protein function. The overall less substitution scores for mutations than WT in our study indicated that these mutations may deteriorate the protein of its overall original function. This provides an opportunity for evolution to select the advantageous changes bestowing bacteria with mutations that could possibly promote its viability and virulence [58,59]. *M.tb* acquires these less favorable mutations which completely or partially eliminate the activity of the associated protein but in turn, make the bacteria more fit to survive against the anti-TB drugs. Similar observations were made for I335T, T262R and T76P mutations of KatG and PncA where the mutations led to substantial deprivation in activity of proteins but in turn, provided resistance to bacteria against two most potent anti-TB drugs namely INH and PZA [58,59]. Therefore, the secondary mutations identified to be resistance conferring in this work could be declared as suspects that despite being less favorable by evolution hold great importance in the survival of the pathogen in stress conditions.

3.3. Analyzing impact of nsSNPs on protein function

***rpoB*:** A total of 517 nsSNPs were studied for their impact on protein function and virulence. Results were obtained for 406 mutations; the remaining 111 mutations were not used due to irregularity in the WT residues at certain codon positions. Out of 406 nsSNPs, 258 (63.5%) were recorded as deleterious, while 148 (36.5%) were predicted as neutral (Supplementary Table 3). The *rpoB* gene mutations are predominantly located within RIF-resistance-determining region (RRDR) corresponding to codons 426 to 452 in *M.tb* [60]. A deeper digging into 258 deleterious nsSNPs brought to light three codon positions, 441, 451 and 456 in RRDR region where four or more AA variants were present. All these mutations, D441F/N/V/Y/A/G/C; H451R/N/Q/C/P/T and S456F/Q/P/W/Y, are known to be associated with RIF drug resistance and were found to be highly deleterious in our analyses.

***inhA*:** A total of 42 nsSNPs were analyzed for their effect on protein function and pathogenicity, of which 37 nsSNPs were obtained by PredictSNP. Among 37 nsSNPs, 13 (35.1%) were predicted as deleterious, while 24 (64.86%) were listed as neutral (Supplementary Table 3). The mutations on the active site of InhA protein through altering its binding with the substrate NADH can disrupt the architecture of the active site and reduce the binding affinity of the drug with InhA. The highly prevalent mutations associated with INH-resistance are found in the active site region (G14, S20, V21, D64, V65, I95, G96, D148, F149, K165, I194, and T196) of InhA [46]. The active site mutations, I21V/T, I95T/P, and I194T were predicted to be deleterious to protein function, the same has been observed in DST [61]. The mutations, I21T, S94A and I95P have been identified to be associated with resistance in both, INH- as well as ETH-resistant clinical isolates [61]. However, S94A and A190S (commonly occurring mutations) were predicted as neutral and did not have any impact on the function of protein.

***katG*:** Among 500 *katG* nsSNPs analyzed for functional impact and pathogenicity, predictions were obtained for 446 nsSNPs. A total of 351 mutations (78.6%) were recorded as deleterious, while 95 (21%) were predicted as neutral (Supplementary Table 3). Resistance causing nsSNPs in *katG* are known to be distributed throughout the coding region. The high number of variants present at a single codon position is indicative of its high mutational propensity in unfavorable conditions providing an escape route for bacteria to survive [62]. In the present work, five such codon positions were

Table 2
Total number of the mutations gathered from multiple sources and pre-processing for selection of mutations for final analysis.

Gene	Total mutations in MycoTRAP-DB	Synonymous mutations	INDELS	Non-synonymous mutations	Final analyzed
rpoB	701	187	36	478	406
inhA	56	11	4	41	37
katG	504	12	24	468	446
pncA	476	5	7	464	402
gyrA	822	552	5	265	258
gyrB	744	442	1	301	246

observed and all the mutations at these positions, N138S/H/D/T, W300G/C/D/I/R, S315L/I/R/T/N/G, W321L/S/R/G/F and W328R/L/C/S/G were predicted to be deleterious with most of them already known to be associated with INH drug resistance [61]. However, the mechanism of resistance in case of W300D, W321G and W328C substitutions has not been explored yet. The deleterious secondary mutations, other than 138, 300, 315, 321 and 328 codon positions, present in the entire coding region of *katG* were also explored for their effects on the protein.

***pncA*:** The functional and pathogenic analysis in *pncA* was initiated with a total of 402 mutations. Based on the consensus results from PredictSNP, 281 (70%) of them were identified as deleterious mutations and 121 (30%) as neutral (Supplementary Table 3). The 281 deleterious mutations included mutations at the iron binding site (D49, H51, H57, H71) and catalytic triad (D8, K96, C138). These results were in concordance with the previous reports that demonstrate the mutations within the active site as the highly detrimental or the resistance conferring mutations [43]. Among them, the variants D8H and C138R were less studied thus offering an opportunity to thoroughly explore their impact.

***gyrA* and *gyrB*:** A total of 271 *gyrA* and 284 *gyrB* mutations were analyzed for their functional and pathogenicity impact. Predictions were obtained for 258 and 246 in *gyrA* and *gyrB,* respectively. The consensus prediction resulted in 63/258 (24.4%) and 64/246 (26%) as deleterious in *gyrA* and *gyrB,* respectively, while 195/258 (75.6%) and 182/246 (74%) were identified as neutral mutations in *gyrA* and *gyrB,* respectively (Supplementary Table 3). As evident from the literature, the QRDR of the *gyrA* (codon 74–113) and *gyrB* (codon 461–499) are hotspot regions [63]. QRDR mutations A90V, S91P and D94G/N/A/H/Y/V/F in *gyrA* and D461N/H, D472H/A, N499D/T in *gyrB* are involved in fluoroquinolone resistance [63,64] and most of them were identified to be deleterious to protein function by our analyses. However, mutations A90V and D94G of *gyrA* were predicted to have no impact on protein function despite being resistant in clinical isolates.

3.4. Structural consequences of nsSNPs

The ΔΔG value calculated as the difference in ΔG score of WT and mutant protein structures is considered as the perfect measure for depicting the impact of single point mutation in changing the stability of the protein [65,66]. Positive and negative values of ΔΔG (kcal mol-1) correspond to increase or decrease in the overall stability of the protein. In the present study, a single point mutation was classified as highly destabilizing (ΔΔG < 0 by all three tools, SDM, STRUM & mCSM), destabilizing (ΔΔG < 0 by any two tools) and stabilizing (ΔΔG > 0 by any two or all three tools). Supplementary Table 4 shows change in protein stability using SDM, STRUM, mCSM web servers in presence of each single point mutation for *rpoB*, *katG*, *inhA*, *pncA*, *gyrA* and *gyrB*.

RpoB*:* A total of 406 nsSNPs were subjected to stability analyses, and predictions were obtained for 299 nsSNPs. Among these, 4 (1.3%) were highly destabilizing, 182 (60.9%) destabilizing and 113 (37.8%) stabilizing mutations. Few mutations were dropped due to the absence of WT residue in crystal structures (RpoB as well as some other genes). The mutations H451R/N/Q/C/P/T and S456F/Q/P/W/Y of RRDR region were observed to reduce the stability of the protein with the exception of D441F/N/V/A/G/C which did not have a destabilizing effect though affecting the protein at functional level. The mildly destabilizing effect in case of all the variants at D441 position might be associated with lower protein fitness penalty thereby retaining the overall fitness of the bacteria in presence of the drug thus further enriching their frequency in the population [62]. In case of *rpoB*, lineage defining mutations, T356I and S394L [67] were predicted to stabilize the protein.

InhA: Among 37 nsSNPs analyzed for structural impact on InhA protein, 21 (56.7%), 9 (24.3%), and 7 (19%) were predicted to be highly destabilizing, destabilizing, and stabilizing, respectively. Highly destabilizing effect on structures was noted for certain well known INH-resistance associated mutations, I21V/T, I95P/T and I194T present on the active site of protein. Other than the active site, K8N and S94A mutations, known to cause resistance widely, were also found as destabilizing in our analysis [61]. Lineage defining polymorphism V78A [67] has no role in resistance however, it was predicted to destabilize the protein structure.

KatG: The structural stability prediction tools revealed a total of 434 mutations, out of which 18 (4.1%), 317 (73%) and 99 (22.8%) mutations were classified as highly destabilizing, destabilizing and stabilizing, respectively. Highly destabilizing effect on protein structure was noted for certain well known INH-resistance associated mutations like N138S, W300G, W321G, amongst others with the exception of S315T and S315N. A very low destabilizing effect was observed in terms of ΔΔG value in case of S315T and S315N mutations. This can be attributed to lower protein fitness penalty based on the similar observation in RpoB [62]. The secondary mutations, W90R, A109V, W328G, A614E, R128G, D142G, T275P and W328G were also recorded as destabilizing, pointing towards their possible candidature to effective drug binding. One of the most commonly occurring and lineage defining mutation R463L [67] was predicted to exhibit a stabilizing effect on the protein structure.

PncA: After the completion of functional analysis, we proceeded with all the 402 mutations to examine their role in inducing the structural changes within the protein. A total of 71 highly destabilizing (17.6%), 295 destabilizing (73%) and 36 stabilizing (8.9%) mutations were obtained. As expected, the prominent residues that form the iron binding site (D49, H51, H57, and H71) and the catalytic triad (C138, D8, K96) were predicted to destabilize the protein with H51N, H71D/E/Q and K96E being the most destabilizing ones. All mutations within these sites displayed the deformity in protein structure except D8V. With negligible structural alteration and even displaying the deleterious functionality earlier, D8V hints at the high impact of active site residues over the protein functionality altogether. Being in a catalytic triad and a prime site facilitating the interaction with PZA, a mutation at D8 seems sufficient to compromise the interaction without destabilizing the overall structure [43].

DNA gyrase: Post functional and pathogenicity analyses, the mutations were subjected to structural analysis which showed 26/227 (11.5%) and 13/228 (5.7%) mutations as highly destabilizing; 143/227 (63%) and 128/228 (56.1%) as destabilizing and 58/227 (25.6%) and 87/228 (38.2%) as stabilizing in GyrA and GyrB, respectively. Highly destabilizing effect on protein structure was noted for L96P (GyrA) and D472A (GyrB) which are prevalent in fluoroquinolone resistance associated mutations [64,68]. The most prevalent QRDR mutations D94G/H/N/A/Y/F/V, G88A or D89N in GyrA and N499D/Y/T/S in GyrB showed very less or no effect on protein stability although these mutations have a remarkable role in fortifying the functionality of the protein. This may be due to the fact that alteration of these key residues does not lead to the deformation of overall structure nonetheless deprives the protein from its function [69]. V125M, a deleterious and highly destabilizing mutation, was observed in the active site region of GyrB pointing towards its possible role in affecting drug binding. Lineage defining mutations, T80A [67] was predicted to increase protein stability and S95T [67] was predicted to have a destabilizing impact on protein.

3.5. Prioritized mutations

For protein-drug interaction studies, mutations were prioritized on the basis of functional and structural effect, prevalence in drug resistant isolates, conservation score, clinically validated, resistance pattern and fold change in drug binding affinity (Supplementary Table 5). Table 3 shows the number of nsSNPs characterized as functionally deleterious or neutral and structurally stabilizing or destabilizing for each gene. The individual tool predictions for the functional and structural impact of prioritized mutations have been provided in Supplementary Tables 6 and 7, respectively. These prioritized mutations were explored for their mechanism of resistance using protein-drug interaction studies.

RpoB: The 22 prioritized mutations included the most prevalent and clinically validated RRDR mutations (D441F/N/V/A/G/C, H451R/N/Q/C/P/T, S456F/Q/P/W/Y) and secondary mutations (A75V, V976M, D1012G and L1128Q) (Fig. 2A). Eleven mutations in RRDR and 4 secondary mutations were predicted to be deleterious as well as destabilizing. The remaining 7 RRDR mutations were deleterious for function and stabilizing with respect to structure, but were considered for further analyses due to their high frequency in drug resistance. The H451D and S456L are the most frequently reported mutations among MDR/XDR strains of *M.tb* across RIF drug resistance spectrum [70,71]. H451D mutant has been described to provide fitness benefits to the pathogen under hypoxic conditions [70]. Mutations in *rpoA*, *rpoB*, and *rpoC* are also common in clinical isolates carrying S531L mutation in rpoB and play a major role in compensating for the fitness loss of the bacteria [10,72].

InhA: Among 11 prioritized mutations, 6 mutations, I21V/T, V65M, I95P/T, and I194T were present on the active site of InhA and had a highly destabilizing and deleterious profile (Fig. 2B). The other mutations, S94A, A190S, G141R, G183R and H265D were secondary mutations. Mutations, S94A and A190S did not have any impact on protein function but reduced its stability largely. G141R, G183R and H265D were considered owing to their significant impact and high prevalence [73].

KatG: The 13 prioritized mutations included clinically validated and highly destabilizing mutations (N138S/D, R128G, D142G, T275P, W300G, W328G); frequently occurring yet uncharacterized destabilizing mutation (W321G, less evidence in literature supporting its resistance pattern); most common and stabilizing/less destabilizing mutation (S315T/N), and other secondary mutations (W90R, A109V, A614E) [25,74,75]. Fig. 3A shows the prioritized primary and secondary mutations in KatG protein. The INH-resistant *M.tb* katG (S315T) variant has been studied to carry fully functional catalase peroxidase activity while decreased INH-oxidase activity [61] makes the bacteria more fit to tackle ROS produced by macrophages and also survive in the presence of isoniazid. Mice studies have revealed that *M.tb* S315T mutation

Table 3
Depiction of nsSNPs as functionally deleterious or neutral and structurally stabilizing or destabilizing as well as the prioritized mutations for each gene.

	Predict SNP			Structural analyses		
Gene	Results obtained	Deleterious	Neutral	Highly destabilizing	Destabilizing	Stabilizing
rpoB	406	258	148	4	182	113
inhA	37	13	24	21	9	7
katG	446	351	95	18	317	99
pncA	402	281	121	71	295	36
gyrA	258	63	195	26	143	58
gyrB	246	64	182	13	128	87

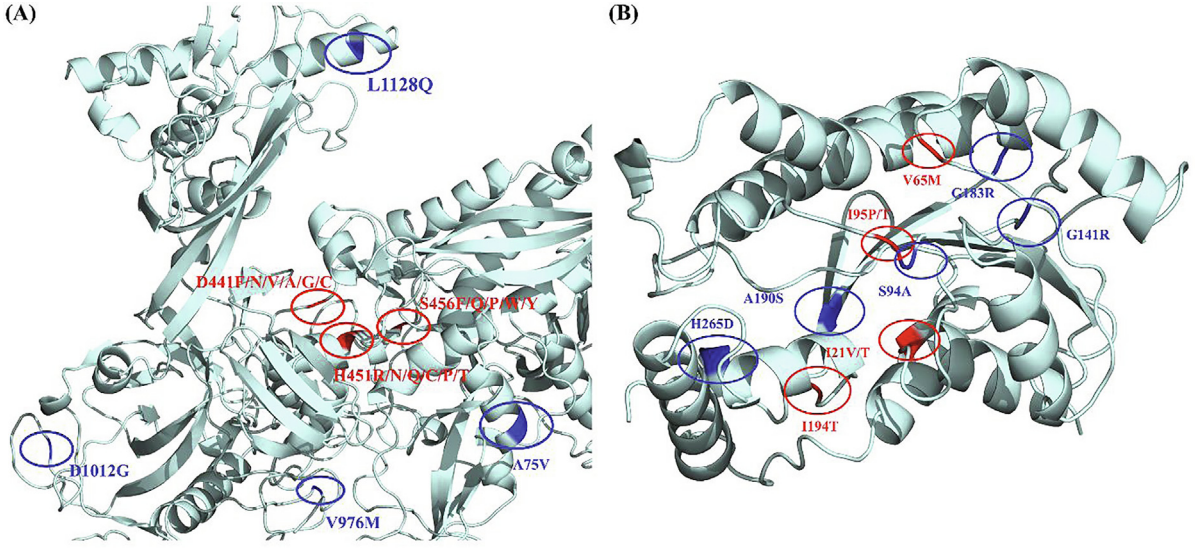

Primary (RRDR): D441F/N/V/A/G/C; H451R/N/Q/C/P/T; S456F/Q/P/W/Y
Secondary: A75V, V976M, D1012G, L1128Q

Primary (Active site) : I21V/T, V65M, I95P/T, I194T
Secondary: S94A, G141R, G183R, A190S, H265D

Fig. 2. Distribution of prioritized primary and secondary mutations in (A) RpoB (B) InhA. Protein is shown in cyan, primary mutations in red and secondary mutations are shown in blue. (For interpretation of the references to colour in this figure legend, the reader is referred to the web version of this article.)

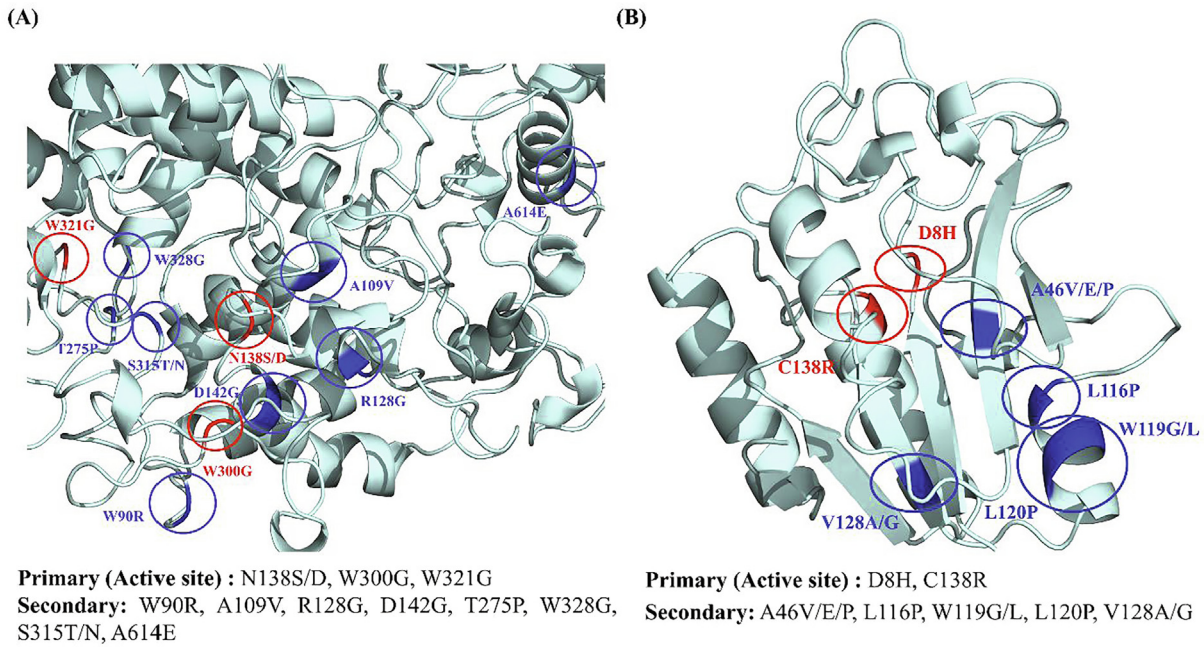

Fig. 3. Distribution of prioritized primary and secondary mutations in (A) KatG (B) PncA. Protein is shown in cyan, primary mutations in red and secondary mutations are shown in blue. (For interpretation of the references to colour in this figure legend, the reader is referred to the web version of this article.)

does not affect bacterial fitness, and it remains fully virulent and highly transmissible [76]. Consequently, the S315T variant is more often found in MDR-TB patients than in INH mono-resistant clinical isolates [77]. Our analysis also found that S315T does not confer any highly destabilizing effect on the protein structure due to which its catalase peroxidase activity is retained and bacteria do not lose their overall fitness.

PncA: Eleven prioritized mutations include the active site mutations like D8H and C138R and secondary mutations A46V/E/P, L116P, W119G/L, L120P, V128A/G predicted as deleterious and destabilizing by structural and functional analyses (Fig. 3B). Among the secondary mutations, L116P, W119G, and L120P were the commonly occurring mutations [78–80]. We observed the presence of several mutations D33A, I6L, S179C and E181R in *pncA* that display a susceptible phenotype against PZA and have also been found in MDR strains of *M.tb* [81–83]. Their existence in MDR strains comes with a low fitness cost as these mutations preserve the protein functionality and at the same time can be suspected for their role in the establishment of MDR. This phenomenon justifies the existence and natural selection of those susceptible mutations which contribute to the drug resistance without compromising the overall fitness of the pathogen.

DNA gyrase: A total of 21 DNA gyrase mutations were considered for further analysis, amongst which A90V, S91P, D94A/G/N, L96P, D461H, D461N, D472A and N499D were QRDR mutations. The other mutations, R309Q, H368Q, R392C [84], R495H, V125M, R212S, R421H, R446C [85], E501V [21], T511N [86–88] and G512R [89–92] were secondary mutations further analyzed in-depth by virtue of their destabilizing and deleterious profiles. Fig. 4A and B represent the primary and secondary mutations prioritized for further studies in DNA gyrase and GyrB ATPase domain respectively. Development of resistance to fluoroquinolones poses the concern of generating XDR-TB strains [85]. A study showed the presence of mutations in *gyrA* and *gyrB* in pre-XDR and XDR *M.tb* strains where all the strains had at least one mutation in QRDR of *gyrA* [93] and *gyrB* [94]. Interestingly, the strains with INH mono-resistance also carried *gyrA* mutations S91P and D94N/Y [93].

3.6. Protein-drug docking and interatomic interactions analyses

The crystal structures and the protein–ligand complexes for WT RpoB, InhA and DNA gyrase (in complex with MFX) obtained after molecular docking had root mean square deviation (RMSD) value of 0 indicating complete alignment of the structures. In case of InhA, the RMSD values obtained after superimposition of WT to I21V and S94A protein–ligand complexes were 0.45 and 0.29, respectively. Table 4 lists molecular docking scores depicting the affinity of WT and mutant proteins, RpoB, InhA, KatG, PncA and DNA gyrase, with the respective drugs. The vibrational entropy values ($\Delta\Delta S_{Vib}$) depicting molecular flexibility and NMA-based values ($\Delta\Delta G$) indicating overall stability of WT and mutant proteins mutations are provided in Table 5.

RpoB: Molecular docking of WT and 22 mutant RpoB structures with RIF was performed to study the effect of mutations on RpoB-RIF binding. Of the total 22 mutations, mutations at all codon positions reduced the binding affinity of RIF to RpoB except in the case of D441Y, S456P and L1128Q where glide docking scores (in kcal/-mol) were more or less similar to WT (-6.5). Large difference in docking scores was observed for S456W (-0.6) followed by D441C (-1.6), H451C (-1.1), H451Q (-1.6), H451T (-1.5) and H451R (-2.0). Docking scores for D441Y, S456P and L1128Q corresponded to −6.3, −6.0 and −6.2 and did not show any significant reduction in binding affinity. The unexplored secondary mutations A75V (-4.3), V976M (-4.7) and D1012G (-4.4) also had reduced docking scores determining their imperative role in drug resistance. A benign mutation I497F had a slightly higher than WT docking score equivalent to −6.9.

The RIF binding pocket is lined by a group of hydrophobic residues, Leu436, Leu458, Gly459 and Ile497 on one side and a polar Gln435 residue at the other end. In WT RpoB, residues participating in H-bonds with RIF include Phe439 (2 bonds) and Arg454 (2 bonds) along with other key residues Gln438, Asp441, His451, Ser456, Asn493 and Ile497 forming hydrophobic network (Fig. 5A). The influence of RRDR mutations at codon positions 441 (D441F/N/V/A/G/C), 451 (H451R/N/Q/C/P/T) and 456 (S456F/Q/P/W/Y) has been studied in length for their

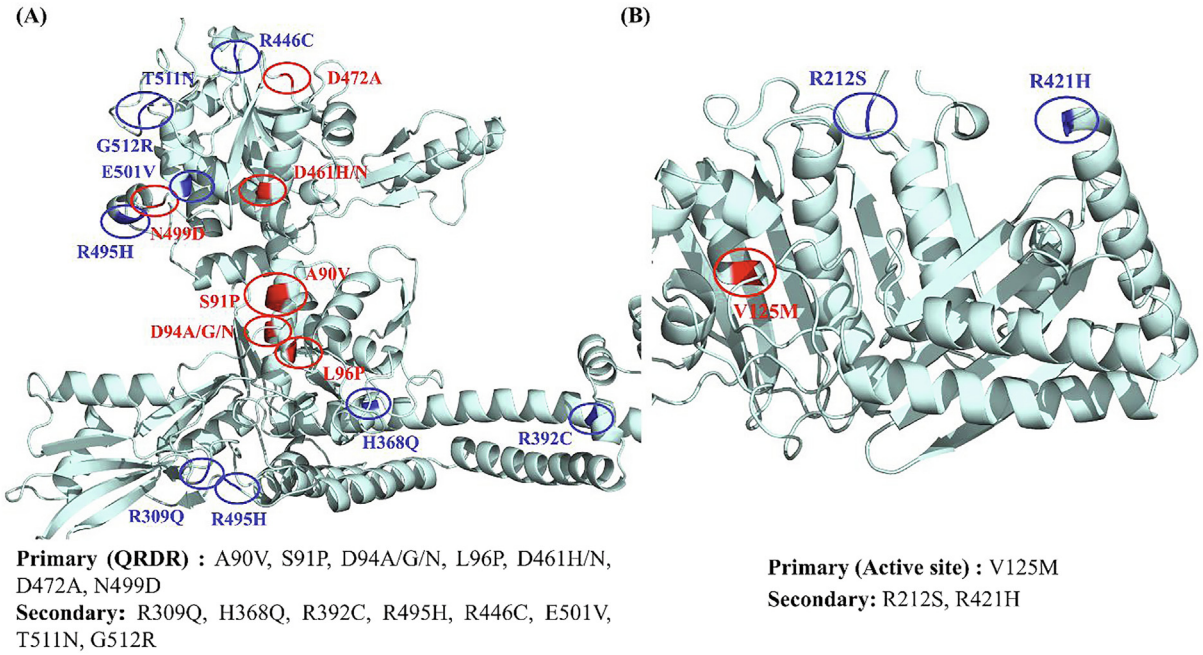

Fig. 4. Distribution of prioritized primary and secondary mutations in (A) DNA gyrase (B) GyrB (ATPase domain). Protein is shown in cyan, primary mutations in red and secondary mutations are shown in blue. (For interpretation of the references to colour in this figure legend, the reader is referred to the web version of this article.)

destabilizing role and reduced binding affinity of RIF to RpoB [95].

In RIF-resistant isolates, 70 to over 90% of RIF-resistant isolates harbor mutations at RpoB codons 441, 451 and 456 [96]. However, the frequencies of SNPs in these three codons are variable in different geographic regions [96]. In case of mutations D441A/C/F/G/N/V/Y, substitution to F/G/V/C resulted in highly reduced binding affinity and moderately reduced in case of A/N/Y. In case of D441A/N mutation, the loss of H-bond with Arg613 and oxygen of RIF in case of substitution to Ala/Asn led to an altered orientation of ligand and disrupted proper drug binding. No change in ligand position was noticed upon replacement of Asp with Tyr, D441Y, still the resistance induced might be due to the low cell wall permeability since this exclusion barrier is responsible for natural resistance of some strains [97,98]. In D441C, the drug formed 3H-bonds but with different residues from the WT, which was due to breakage of H-bonds with Phe439 and Arg613 and a drastic reduction in binding affinity for RIF. The D441C substitution changed the position of RIF and exposed it to the solvent in response to a significant reduction in hydrophobic interacting residues further making the binding pocket inaccessible to RIF. In case of D441F mutation, decreased molecular flexibility ($\Delta\Delta S_{Vib}$ ENCOM −0.049), alterations in H-bonds as well as decreased hydrophobicity along with large conformational change in the ligand was noticed which restricted the ligand from reaching the catalytic site. The D441V mutation increased the molecular flexibility ($\Delta\Delta S_{Vib}$ ENCOM 0.281), the H-bond between carbonyl of RIF and Arg454 shifted to H-bond between oxygen and Arg454 leading to ligand disorientation in the binding pocket and a considerable decrease in ligand binding affinity. All the H-bonds were lost in D441G mutation which did not let the ligand to reach the depth of the binding pocket and moved it towards the surface which is also reflected from the highly reduced docking score as compared to WT.

In RpoB protein, His451 is the most important β-subunit residue, involved in RNAP/RIF complex, through hydrogen bonding with the RIF ring system oxygen atoms as determinants. His451 mutants are considered "affinity mutants" since they interfere with crucial protein polar/hydrophobic RNAP/RIF interactions [99]. The substitutions in codon 451 (H/Y/D/R/L/P) in RpoB are very common in *M.tb* clinical isolates highly resistant to RIF [100–102]. Substitution of His to any other AA is quite rare as it is not well physiologically favored due to its chemical properties [103]. The mutation of His451 to D/R/Y has been well studied for the mechanism of resistance [104–106]. However, the other variants identified to be deleterious to function and destabilizing to structure by our analysis have not been well explored. In the case of H451C/Q/T mutation, the weak interatomic interactions in the mutants lead to an increase in the flexibility of the native protein reaching 0.369, 0.307 and 0.467 ($\Delta\Delta S_{Vib}$ ENCOM) for H451C/Q/T, respectively. A considerable change in ligand orientation in the binding pocket of RpoB and loss of H-bonds was seen making RIF exposed to the solvent and leading to much decrease in docking score as compared to WT and other mutations. An overlap in the conformation of ligand to that of WT was found in H451N mutation which is also evident from their almost similar docking scores. The residues in H451P mutation are changing from polar to hydrophobic which resulted in loss of H-bonds with Arg613 and key residue Phe439 and thus change in ligand orientation and an increase in flexibility ($\Delta\Delta S_{Vib}$ ENCOM 0.682) of the native protein.

Mutation at codon 456 is another predominant alteration as reported in previous studies [95,96]. At Ser456, W/F/Q are most frequently occurring substitutions [96] and their mechanisms of resistance have already been explored. Amongst the other variants (S456P/Y), in S456P since Ser is known to mimic Pro, this mutation induced hardly any change in conformation of ligand which is also clear from its similar docking score to WT along with slight increase in molecular flexibility ($\Delta\Delta S_{Vib}$ ENCOM 0.074). In the case of S456Y mutation, the single aromatic ring of RIF moved in a direction opposite to WT and formed H-bond with Arg493. All the H-bonds formed amid WT RpoB and RIF were lost leading to a considerable decrease in the docking score as compared to WT.

Amongst the unexplored secondary mutations, in the A75V mutation, only one H-bond, with Arg454, was retained in contrast to 4H-bonds in WT protein–ligand complex (Fig. 5B). Val contains two non-hydrogen substituents i.e., two carbons which increases the bulkiness near the protein backbone resulting in confined

Table 4
Molecular docking scores depicting the affinity of WT proteins and their mutant forms with the respective drugs.

Protein	Drug	Mutation	Glide score (kcal/mol)
RpoB	Rifampicin	WT	−6.5
		A75V	−4.3
		D441A	−4.1
		D441C	−1.6
		D441F	−1.7
		D441G	−2.0
		D441N	−6.1
		D441V	−3.6
		D441Y	−6.3
		H451C	−1.1
		H451N	−5.4
		H451P	−4.0
		H451Q	−1.6
		H451R	−2.0
		H451T	−1.5
		S456F	−3.8
		S456P	−6.0
		S456Q	−4.3
		S456W	−0.6
		S456Y	−4.1
		V976M	−4.7
		D1012G	−4.4
		L1128Q	−6.2
		I497F (Benign)	−6.9
InhA	INH-NAD	WT	−16.8
		I21T	−16.6
		I21V	−13.5
		V65M	−10.2
		S94A	−14.1
		I95T	−15.9
		I95P	−14.9
		G141R	−17.0
		G183R	−15.7
		A190S	−8.2
		I194T	−13.0
		H265D	−17.0
		V78A (Benign)	−17.2
KatG	Isoniazid	WT	−5.0
		W90R	−4.5
		A109V	−4.1
		R128G	−4.5
		N138S	−4.8
		N138D	−4.9
		D142G	−4.9
		T275P	−4.2
		W300G	−4.5
		S315T	−4.7
		S315N	−4.9
		W321G	−4.4
		W328G	−4.9
		A614E	−5.0
		A110V (Benign)	−5.1
PncA	Pyrazinamide	WT	−4.7
		D8H	−4.7
		A46V	−4.4
		A46E	−4.4
		A46P	−4.6
		L116P	−4.6
		W119G	−4.5
		W119L	−4.4
		L120P	−4.4
		V128A	−4.7
		V128G	−4.6
		C138R	−4.7
		A134D (Benign)	−4.8
DNA gyrase	Ofloxacin	WT	−7.3
	Moxifloxacin	WT	−6.8
	Ciprofloxacin	WT	−8.2
	Levofloxacin	WT	−4.8
	Ofloxacin	A90V	−5.0
	Moxifloxacin	A90V	−4.8
	Ciprofloxacin	A90V	−4.0
	Levofloxacin	A90V	−3.7
	Ofloxacin	S91P	−4.6

Table 4 (*continued*)

Protein	Drug	Mutation	Glide score (kcal/mol)
	Moxifloxacin	S91P	−3.3
	Ciprofloxacin	S91P	−4.0
	Levofloxacin	S91P	−2.9
	Ofloxacin	D94A	−6.0
	Moxifloxacin	D94A	−4.8
	Ciprofloxacin	D94A	−3.9
	Levofloxacin	D94A	−3.8
	Ofloxacin	D94G	−4.3
	Moxifloxacin	D94G	−4.9
	Ciprofloxacin	D94G	−4.6
	Levofloxacin	D94G	−3.5
	Ofloxacin	D94N	−3.3
	Moxifloxacin	D94N	−4.3
	Ciprofloxacin	D94N	−6.6
	Levofloxacin	D94N	−3.5
	Ofloxacin	L96P	−3.4
	Moxifloxacin	L96P	−5.2
	Ciprofloxacin	L96P	−4.8
	Levofloxacin	L96P	−3.2
	Ofloxacin	R309Q	−3.3
	Moxifloxacin	R309Q	−6.7
	Ciprofloxacin	R309Q	−4.7
	Levofloxacin	R309Q	−3.6
	Ofloxacin	H368Q	−4.8
	Moxifloxacin	H368Q	−5.8
	Ciprofloxacin	H368Q	−6.0
	Levofloxacin	H368Q	−3.1
	Ofloxacin	R392C	−5.4
	Moxifloxacin	R392C	−5.3
	Ciprofloxacin	R392C	−6.7
	Levofloxacin	R392C	−2.9
	Ofloxacin	R495H	−3.5
	Moxifloxacin	R495H	−3.2
	Ciprofloxacin	R495H	−4.2
	Levofloxacin	R495H	−3.6
	Ofloxacin	R446C	−4.3
	Moxifloxacin	R446C	−4.7
	Ciprofloxacin	R446C	−5.8
	Levofloxacin	R446C	−3.3
	Ofloxacin	D461H	−4.9
	Moxifloxacin	D461H	−3.7
	Ciprofloxacin	D461H	−4.3
	Levofloxacin	D461H	−4.1
	Ofloxacin	D461N	−3.6
	Moxifloxacin	D461N	−2.8
	Ciprofloxacin	D461N	−4.3
	Levofloxacin	D461N	−4.3
	Ofloxacin	D472A	−5.1
	Moxifloxacin	D472A	−5.2
	Ciprofloxacin	D472A	−6.3
	Levofloxacin	D472A	−3.7
	Ofloxacin	N499D	−2.8
	Moxifloxacin	N499D	−5.4
	Ciprofloxacin	N499D	−6.1
	Levofloxacin	N499D	−4.0
	Ofloxacin	E501V	−2.9
	Moxifloxacin	E501V	−3.4
	Ciprofloxacin	E501V	−4.9
	Levofloxacin	E501V	−3.2
	Ofloxacin	T511N	−4.2
	Moxifloxacin	T511N	−4.7
	Ciprofloxacin	T511N	−4.6
	Levofloxacin	T511N	−3.5
	Ofloxacin	G512R	−2.1
	Moxifloxacin	G512R	−2.2
	Ciprofloxacin	G512R	−4.8
	Levofloxacin	G512R	−3.5
	Ofloxacin	S95T (Benign)	−7.3
	Moxifloxacin	S95T (Benign)	−6.8
	Ciprofloxacin	S95T (Benign)	−8.2
	Levofloxacin	S95T (Benign)	−4.8
GyrB (Nter), ATPase domain	Ofloxacin	WT	−5.5
	Moxifloxacin	WT	−5.7
	Ciprofloxacin	WT	−5.0
	Levofloxacin	WT	−3.7

(*continued on next page*)

Table 4 (*continued*)

Protein	Drug	Mutation	Glide score (kcal/mol)
	Ofloxacin	V125M	−5.5
	Moxifloxacin	V125M	−2.7
	Ciprofloxacin	V125M	−7.6
	Levofloxacin	V125M	−3.6
	Ofloxacin	R212S	−4.0
	Moxifloxacin	R212S	−4.1
	Ciprofloxacin	R212S	−4.4
	Levofloxacin	R212S	−1.1
	Ofloxacin	R421H	−6.5
	Moxifloxacin	R421H	−5.6
	Ciprofloxacin	R421H	−6.5
	Levofloxacin	R421H	−2.2

Table 5
Vibrational entropy values depicting molecular flexibility and ΔΔG values indicating overall stability of WT and mutant proteins mutations.

Protein	Mutation	NMA Based Predictions (ΔΔG ENCoM in kcal/mol)	Outcome	$\Delta\Delta S_{Vib}$ ENCoM (kcal.mol-1.K-1)	Molecule flexibility Outcome
RpoB	A75V	−0.05	Destabilizing	0.063	Increase
	D441F	0.039	Destabilizing	−0.049	Decrease
	D441N	−0.181	Destabilizing	0.227	Increase
	D441V	−0.225	Destabilizing	0.281	Increase
	D441Y	0.313	Destabilizing	−0.391	Decrease
	D441A	−0.252	Destabilizing	0.315	Increase
	D441G	−0.469	Destabilizing	0.586	Increase
	D441C	−0.197	Destabilizing	0.246	Increase
	H451R	−0.031	Destabilizing	0.039	Increase
	H451N	−0.563	Destabilizing	0.703	Increase
	H451Q	−0.245	Destabilizing	0.307	Increase
	H451C	−0.295	Destabilizing	0.369	Increase
	H451P	−0.545	Destabilizing	0.682	Increase
	H451T	−0.373	Destabilizing	0.467	Increase
	S456F	0.273	Destabilizing	−0.342	Decrease
	S456Q	0.098	Destabilizing	−0.123	Decrease
	S456P	−0.059	Destabilizing	0.074	Increase
	S456W	0.372	Destabilizing	−0.465	Decrease
	S456Y	0.278	Destabilizing	−0.348	Decrease
	V976M	0.397	Destabilizing	−0.496	Decrease
	D1012G	−0.161	Destabilizing	0.201	Increase
	L1128Q	−0.266	Destabilizing	0.332	Increase
InhA	I21V	−0.344	Destabilizing	0.43	Increase
	I21T	−0.282	Destabilizing	0.352	Increase
	V65M	0.028	Destabilizing	−0.035	Decrease
	S94A	−0.242	Destabilizing	0.303	Increase
	I95P	−0.498	Destabilizing	0.623	Increase
	I95T	−0.272	Destabilizing	0.339	Increase
	G141R	0.613	Stabilizing	−0.767	Decrease
	G183R	0.08	Destabilizing	−0.1	Decrease
	A190S	0.225	Destabilizing	−0.281	Decrease
	I194T	−0.085	Destabilizing	0.106	Increase
	H265D	−0.073	Destabilizing	0.092	Increase
KatG	W90R	−0.664	Destabilizing	0.83	Increase
	A109V	0.216	Destabilizing	−0.27	Decrease
	R128G	−0.997	Destabilizing	1.246	Increase
	N138S	0.102	Destabilizing	−0.127	Decrease
	N138D	0.138	Destabilizing	−0.172	Decrease
	D142G	−0.577	Destabilizing	0.721	Increase
	T275P	−0.03	Destabilizing	0.039	Increase
	W300G	−2.195	Destabilizing	2.744	Increase
	S315T	0.345	Destabilizing	−0.432	Decrease
	S315N	0.164	Destabilizing	−0.205	Decrease
	W321G	−1.194	Destabilizing	1.492	Increase
	W328G	−1.606	Destabilizing	2.008	Increase
	A614E	0.142	Destabilizing	−0.178	Decrease
PncA	D8H	0.128	Destabilizing	−0.16	Decrease
	A46V	0.2	Destabilizing	−0.249	Decrease
	A46P	0.203	Destabilizing	−0.254	Decrease
	A46E	0.148	Destabilizing	−0.185	Decrease
	L116P	−0.833	Destabilizing	1.041	Increase
	L120P	−0.274	Destabilizing	0.342	Increase
	W119G	−1.153	Destabilizing	1.442	Increase
	W119L	−0.711	Destabilizing	0.889	Increase

Table 5 (*continued*)

Protein	Mutation	NMA Based Predictions (ΔΔG ENCoM in kcal/mol)	Outcome	$\Delta\Delta S_{Vib}$ ENCoM (kcal.mol-1.K-1)	Molecule flexibility Outcome
	V128A	−0.43	Destabilizing	0.537	Increase
	V128G	−0.738	Destabilizing	0.922	Increase
	C138R	0.372	Destabilizing	−0.465	Decrease
	S67L(susceptible)	0.22	Destabilizing	−0.274	Decrease
GyrA	A90V	0.238	Destabilizing	−0.298	Decrease
	A90S	−0.016	Destabilizing	0.019	Increase
	A90T	0.128	Destabilizing	−0.16	Decrease
	A90G	0.034	Destabilizing	−0.043	Decrease
	A90C	0.059	Destabilizing	−0.073	Decrease
	S91P	−0.053	Destabilizing	0.066	Increase
	S91A	−0.103	Destabilizing	0.129	Increase
	D94G	0.015	Destabilizing	−0.019	Decrease
	D94H	0.237	Destabilizing	−0.297	Decrease
	D94N	0.004	Destabilizing	−0.005	Decrease
	D94V	0.080	Destabilizing	−0.100	Decrease
	D94A	−0.013	Destabilizing	0.016	Increase
	D94F	0.230	Destabilizing	−0.287	Decrease
	D94Y	0.375	Destabilizing	−0.469	Decrease
	L96P	−0.358	Destabilizing	0.447	Increase
	R309Q	0.042	Destabilizing	−0.053	Decrease
	H368Q	−0.287	Destabilizing	0.358	Increase
	R392C	−0.149	Destabilizing	0.186	Increase
	R392L	−0.086	Destabilizing	0.107	Increase
	R495H	−0.115	Destabilizing	0.144	Increase
	S95T	−0.034	Destabilizing	0.043	Increase
GyrB	V125M	0.399	Destabilizing	−0.499	Decrease
	R212S	−0.619	Destabilizing	0.773	Increase
	R421H	0.026	Destabilizing	−0.032	Decrease
	R446C	−0.557	Destabilizing	0.697	Increase
	D461N	−0.037	Destabilizing	0.046	Increase
	D461H	−0.045	Destabilizing	0.056	Increase
	D472A	−0.126	Destabilizing	0.157	Increase
	D472H	−0.07	Destabilizing	0.088	Increase
	D472N	−0.107	Destabilizing	0.134	Increase
	N499D	−0.048	Destabilizing	0.06	Increase
	N499Y	0.23	Destabilizing	−0.288	Decrease
	N499T	0.058	Destabilizing	−0.072	Decrease
	N499S	0.021	Destabilizing	−0.027	Decrease
	T500A	−0.088	destabilizing	0.110	Increase
	T500N	−0.085	destabilizing	0.106	Increase
	E501V	−0.134	Destabilizing	0.168	Increase
	E501D	−0.318	Destabilizing	0.397	Increase
	A504V	0.307	Destabilizing	−0.384	Decrease
	T511N	−0.247	Destabilizing	0.309	Increase
	G512R	0.597	Stabilizing	−0.746	Decrease
	M291I	−0.348	Destabilizing	0.435	Increase

movement of nearby residues. So, under the influence of Val, protein flexibility ($\Delta\Delta S_{Vib}$ ENCOM 0.063) increased and the position of ligand within the binding site got disturbed further affecting the binding capacity of ligand to the protein. In case of V976M mutation, substitution from Val to Met disturbed the interactions with neighboring protein residues as a result of which the ligand, after entering the pocket, rotated and moved in an opposite direction from the binding pocket and thus low ligand affinity for the protein. As is evident from Fig. 5C, in the case of mutation from Asp (polar) to Gly (non-polar) at position 1012, a H-bond with Arg454, the key residue of binding pocket, is broken which forced the ligand to move away from the hydrophobic binding pocket subsequently leading to reduced affinity of RIF for RpoB thus increasing the flexibility of molecule ($\Delta\Delta S_{Vib}$ ENCOM 0.201). The L1128Q mutation did not largely impact ligand binding and all the H-bonds and hydrophobic interactions were retained except that the mutation pushed the ligand marginally inside the binding pocket (Fig. 5D) but an overall increase in randomness ($\Delta\Delta S_{Vib}$ ENCOM 0.332) in the protein structure was observed.

InhA: To investigate the impact of mutations on the binding of activated INH with InhA i.e., INH-NAD adduct, molecular docking was performed. All the mutant structures showed reduced docking scores (in kcal/mol) as compared to WT score, −16.8. Mutations I21V (-13.5), S94A (-14.1), I95P (-14.9), I95T (-15.9), G183R (-15.7) and I194T (-13.0) resulted in a low-affinity INH-NAD binding. A large difference in binding affinity was observed for V65M (-10.2) and A190S (-8.2). The score for I21T (-16.6), G141R (-17.0) and H265D (-17.0) was more or less comparable to the WT. The docking score for the benign mutation V78A was more than WT and corresponded to −17.2.

The strong binding in WT is the result of 6H-bonds and 15 hydrophobic interactions formed between WT InhA and INH-NAD (Fig. 6A). INH-NAD is buried in a largely hydrophobic binding pocket in InhA protein thus changes induced in hydrophobicity by certain mutations might have been responsible for decreased binding affinity of activated INH. In I21T, a loss of few hydrophobic residues owing to the weakly polar nature of Thr as well as bulky side chain restricting the movement of neighboring backbone residues was observed. In case of I21V (active site) mutation, though Ile and Val are equally hydrophobic, minor differential changes were observed in terms of interactions with the adjacent residues but an overall increase in randomness ($\Delta\Delta S_{Vib}$ ENCOM 0.430) in the protein structure was seen. Ile is known to be highly important in protein–ligand binding. Val at the same time has high frequency

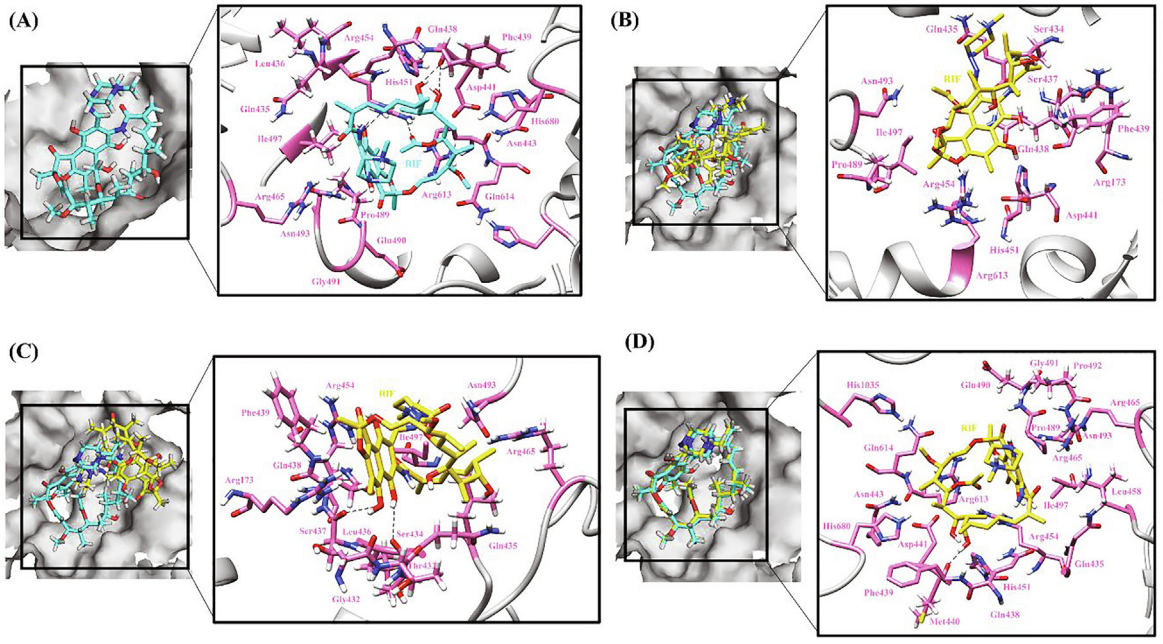

Fig. 5. Hydrogen bonding and hydrophobic interactions in RpoB-RIF complex. (A) WT (B) A75V (C) D1012G (D) L1128Q. The left panel is a view of the drug inside the binding pocket of protein and the right panel illustrates protein residues interacting with the drug. RIF is shown in cyan in WT and yellow in mutants. Hydrogen bonding and hydrophobic residues are shown in pink. Black dashed lines represent hydrogen bonds. (For interpretation of the references to colour in this figure legend, the reader is referred to the web version of this article.)

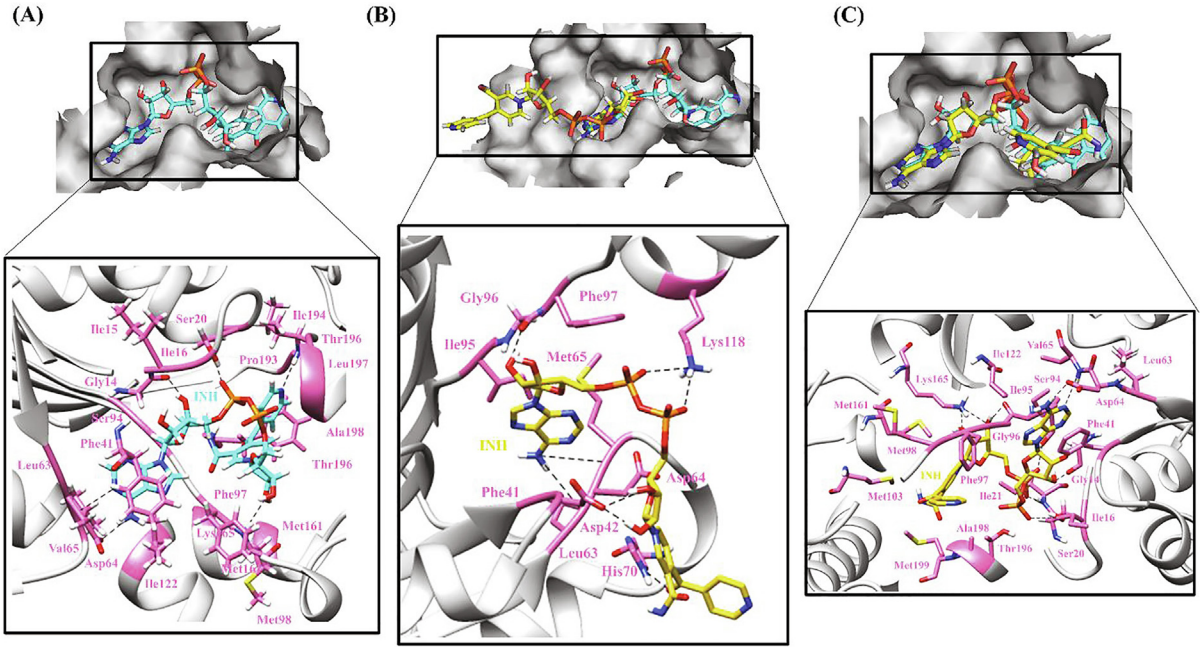

Fig. 6. Hydrogen bonding and hydrophobic interactions in InhA-INH-NAD complex. (A) WT (B) V65M (C) A190S. The top panel is a view of the drug inside the binding pocket of protein and the bottom panel illustrates protein residues interacting with the drug. INH-NAD is shown in cyan in WT and yellow in mutants. Hydrogen bonding and hydrophobic residues are shown in pink. Black dashed lines represent hydrogen bonds. (For interpretation of the references to colour in this figure legend, the reader is referred to the web version of this article.)

of occurrence near the ligand [107] in absence of which INH-NAD ligand changed its coordinates with respect to its conformation in WT leading to low-affinity ligand binding. Major loss of interatomic interactions was observed in I194T ($\Delta\Delta S_{Vib}$ ENCOM 0.106) as compared to I95T ($\Delta\Delta S_{Vib}$ ENCOM 0.339) depicting its upper hand in modifying the environment inside the binding pocket. In case of I194T, a H-bond formed between Ile194 and INH-NAD was no longer seen and the ligand moved in direction opposite to that in WT on encountering Thr instead of Ile. In case of I95P, replacement of Ile to Pro did not change the H-bonds and hydrophobic interactions however increased the solvent exposure due to which the position of ligand got disturbed reducing its

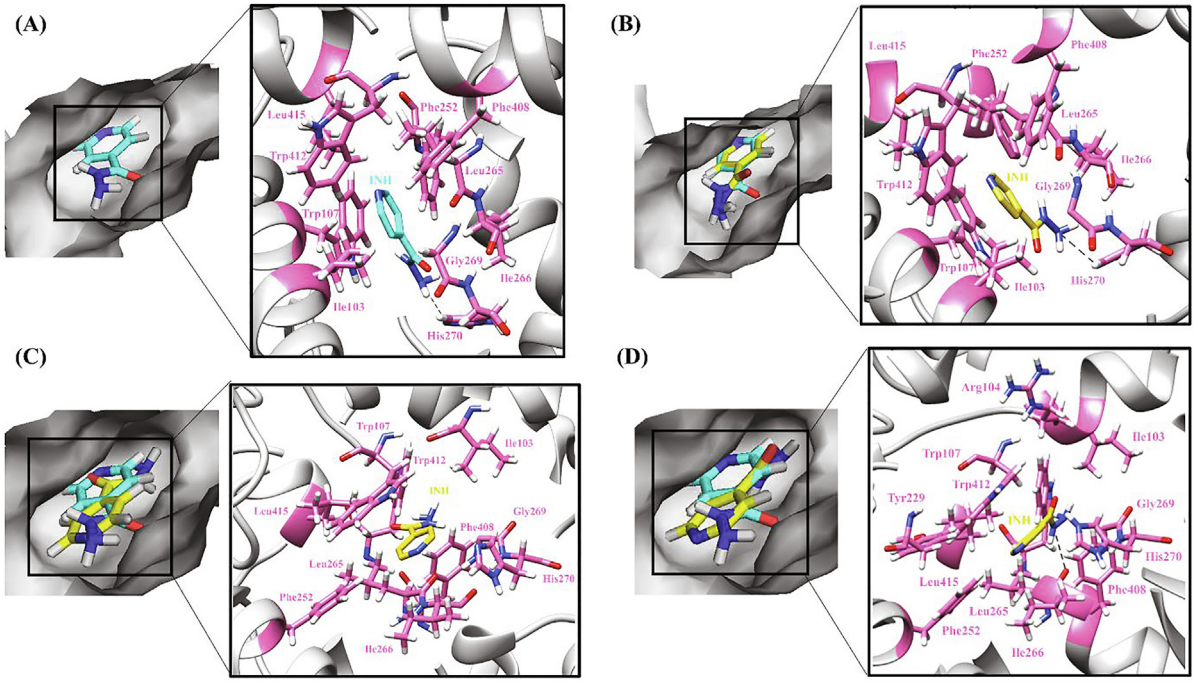

Fig. 7. Hydrogen bonding and hydrophobic interactions in KatG-INH complex. (A) WT (B) W90R (C) A109V (D) W321G. The left panel is a view of the drug inside the binding pocket of protein and the right panel illustrates protein residues interacting with the drug. INH is shown in cyan in WT and yellow in mutants. Hydrogen bonding and hydrophobic residues are shown in pink. Black dashed lines represent hydrogen bonds. (For interpretation of the references to colour in this figure legend, the reader is referred to the web version of this article.)

strength of binding to InhA. In another active site mutation V65M, substitution of Val with Met accompanied development of H-bonds with adjoining residues which consequently augmented rigidity ($\Delta\Delta S_{Vib}$ ENCOM −0.035) in the affected area and narrowing of the binding pocket. A large reduction in hydrophobicity and breaking of the H-bond with Val and formation with Met in the V65M mutation induced a huge conformational change owing to which the ligand did not reach the hydrophobic pocket and settled on the surface of protein (Fig. 6B).

Mutation S94A increased protein flexibility ($\Delta\Delta S_{Vib}$ ENCOM 0.303) by change in interatomic interactions, specifically formation of hydrophobic interactions owing to the hydrophobic nature of Ala. With no Ser at 94 position, the ligand rotated at phosphate linkages and changed its course to reach the binding pocket compromising interactions with the neighboring residues and did not fit well inside the binding pocket. S94A mutation has been shown to reduce the binding of INH-NADH and increase the IC50 and Ki by 17 and 30 times respectively as compared to WT [108]. In secondary mutations, G141R and G183R, substitution from Gly (smallest AA) to Arg (polar) led to the formation of a few new interactions with the neighboring residues which made the affected area quite stable. Also being present away from the binding pocket, the resulting change in flexibility did not influence ligand binding much compared with WT as is reflected from the overlapping coordinates of ligands in WT and mutant protein–ligand complexes. In the A190S mutation, overall molecular flexibility was decreased ($\Delta\Delta S_{Vib}$ ENCOM −0.281) due to the change from hydrophobic residue Ala to Ser which is a polar AA with tendency to form H-bonds. A considerable rotation was seen in INH-NAD from its position in WT since the ligand on coming across Ser got exposed to solvent and did not fully reach the binding pocket (Fig. 6C). Exchange of His with any AA is mostly non-favorable as its pKa is very close to that of physiological pH and thus the binding capacity of ligand was not hampered and docking score observed in H265D mutation (-17.0 kcal/mol) was similar to WT.

KatG: Molecular docking of WT KatG and 13 mutant structures with INH was performed to study the effect of mutations on KatG-INH binding. As compared to WT (-5.0), R128G (-4.5), T275P (-4.2), W300G (-4.5) and W321G (-4.4) mutants had lesser docking scores (in kcal/mol) representing their reduced INH binding affinity. The scores for N138S (-4.8), N138D (-4.9), D142G (-4.9), W328G (-4.9), S315T (-4.7), S315N (-4.9) and A614E (-5.0) were more or less comparable to the WT. The docking scores of the unexplored secondary mutations, W90R (-4.5) and A109V (-4.1) determine their possible distinctiveness in minimizing the INH-oxidase activity of KatG and further leading to resistance against INH. Almost similar to WT docking score was obtained in case of benign mutation A110V (-5.10).

The strong binding affinity of INH to WT KatG protein can be explained by 8 hydrophobic network forming residues present around the ligand (INH) along with the 1H-bond between His270 and NH2 group of INH and one pi-pi (Trp107) interaction (Fig. 7A). In the mutations, T275P and D142G, Thr and Asp are changing to non-polar and neutral residues known to induce flexibility ($\Delta\Delta S_{Vib}$ ENCOM 0.039) and ($\Delta\Delta S_{Vib}$ ENCOM 0.721) in protein, respectively. In the case of T275P, the mutant residues formed an intricate network of interactions with surrounding AAs changing the shape of the binding pocket and leading to a loss in INH interactions which certainly changed the orientation of INH thereby affecting its absolute binding and activation.

Substitution of a nonpolar AA (Trp) with a positively charged residue (Arg) as in matter of W90R, led to a huge loss of interactions with neighboring residues and an increase in local flexibility ($\Delta\Delta S_{Vib}$ ENCOM 1.246) although there was no change in orientation of the ligand (Fig. 7B). In the case of A109V mutant structure, more hydrophobic and hydrogen interactions were observed to be made by Val with the surrounding residues along with the increase

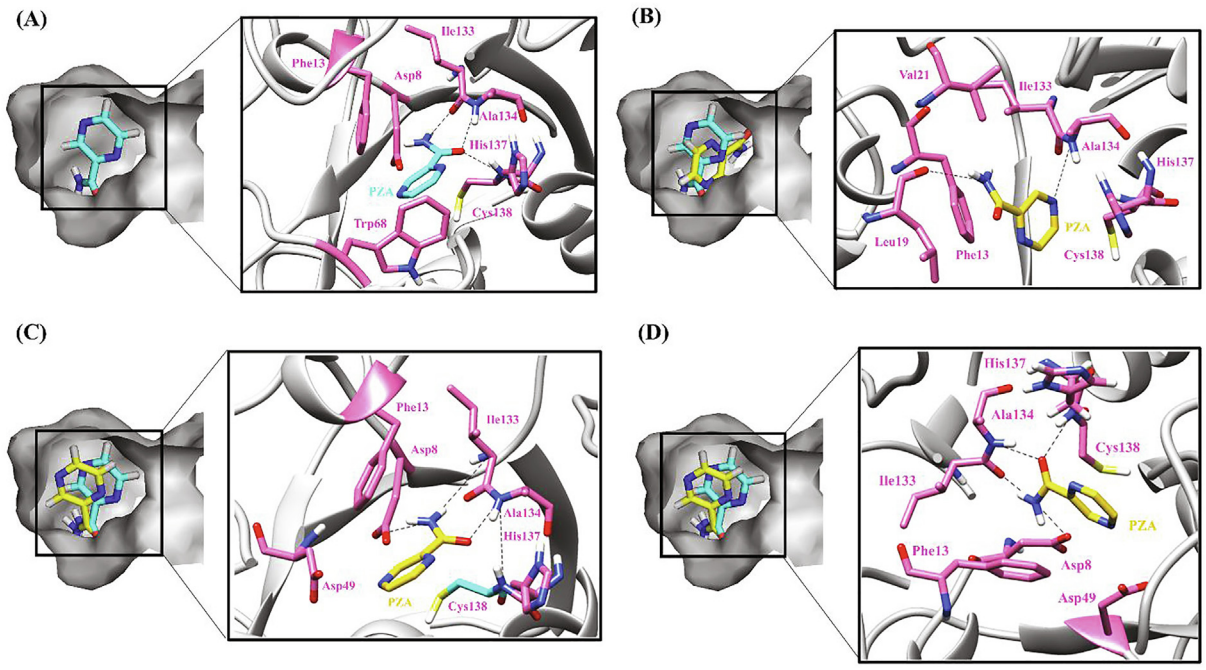

Fig. 8. Hydrogen bonding and hydrophobic interactions in PncA-PZA complex. (A) WT (B) W119L (C) A46E (D) A46V. The left panel is a view of the drug inside the binding pocket of protein and the right panel illustrates protein residues interacting with the drug. PZA is shown in cyan in WT and yellow in mutants. Hydrogen bonding and hydrophobic residues are shown in pink. Black dashed lines represent hydrogen bonds. (For interpretation of the references to colour in this figure legend, the reader is referred to the web version of this article.)

in rigidity of nearby area ($\Delta\Delta S_{Vib}$ ENCOM −0.270) which can result in the constriction or change in the shape of binding pocket [109]. Furthermore, the ligand was observed to adhere away from the hydrophobic core of the binding pocket subsequently leading to its improper binding and activation (Fig. 7C).

In context with the mutations R128G, W300G and W321G, the WT residues are being replaced by small AA Gly which is aliphatic and devoid of any side chains which is thought as a contributory factor for the partial rotation of drug inside the enzyme binding pocket. Moreover, the replacement of an aromatic and high molecular weight AA Trp with Gly as in the case of W300G and W321G (Fig. 7D) mutant models led to the depletion of necessary interactions with the surrounding residues required to stabilize the binding pocket. All these variations collectively contributed to disrupting the ligand binding affinity, by changing its orientation away from the catalytic site to a more solvent exposed area. These mutations are therefore associated with low disturbances in drug binding and less INH resistance (0.5–1 μg/ml) [110,111]. However, more experimental studies are needed to confirm this hypothesis.

In the mutation A614E, the codon position Ala614 is localized near the C-ter domain of KatG. This conserved codon position appears to mutate and code marginally favorable negatively charged AA Glu to defend bacteria against INH stress. The substitution brings challenges to the protein in terms of reduction in halogen and hydrogen bonds in mutated structure but subsequently the increment in the number of new hydrophobic and weak hydrogen interactions seems to compensate for the onsite loss. This somehow favors the drug to properly adjust inside the binding pocket and thus forms a stable protein-drug complex which explains this substitution as functionally deleterious and overall, structurally destabilizing yet not hampering binding affinity of INH much as compared to the WT. S315T and S315N mutations turned out to be deleterious to protein function but had a stabilizing and mildly destabilizing effect on protein structure respectively. Still, they are most frequently appearing mutations in the drug resistant isolates. Both the mutations increased the interactions of mutated residue with the neighboring AAs which accompanied stability in the enzyme binding pocket. Apart from the minor alterations in the position of nearby residues, a prominent differential change in orientation of the ligand or conformation of the binding pocket was not seen between WT and mutant protein–ligand complexes since this was a conservative substitution. Still the resistance induced by substitution of Ser with Thr at codon position 315 might be due to some other mechanisms like interference in the electron-transfer chain triad and proposed mechanism of threonine steric constraint further helping this mutation in reducing INH-oxidase activity and causing resistance [112]

PncA: Docking studies performed to assess the impact of mutations on protein-drug binding exhibited low ligand binding propensity in the case of all the mutations except D8H, V128A and C138R. The docking score (in kcal/mol) for the WT was found to be −4.7 while the score in case of mutant protein–ligand complexes ranged from −4.4 to −4.7. The benign mutation A134D had higher docking score of −4.8 as compared to the WT.

Hydrophobic interactions are key driving factors in maintaining the conformational integrity of the binding pocket in PncA which facilitates prompt activation of PZA. The residues, Asp8, Lys96 and Cys138 form catalytic triad in PncA where Cys138, upon activation by Asp8, initiates the covalent catalysis by acting as a nucleophile. Lys96 on the other hand stabilizes either the Asp8 or the thiolated form of Cys138 during the catalysis mechanism [113]. The Fe^{+2} ion has a catalytic role than a structural one and is coordinated inside the active site by residues His57, His71, and His137 [43].

In case of WT PncA, besides the hydrophobic environment, the residues Ala134 and Cys138 form two H-bonds with the carbonyl oxygen atom and Ile 133 forms one with the terminal amino group of PZA thus contributing to the stability of the complex. Furthermore, the polar interactions between Asp8, His71 and His137 of the protein and PZA together with the pi-pi interaction between aromatic Trp68 and aromatic ring of PZA reinforce the integrity of the drug-protein complex and assist the PZA activation (Fig. 8A).

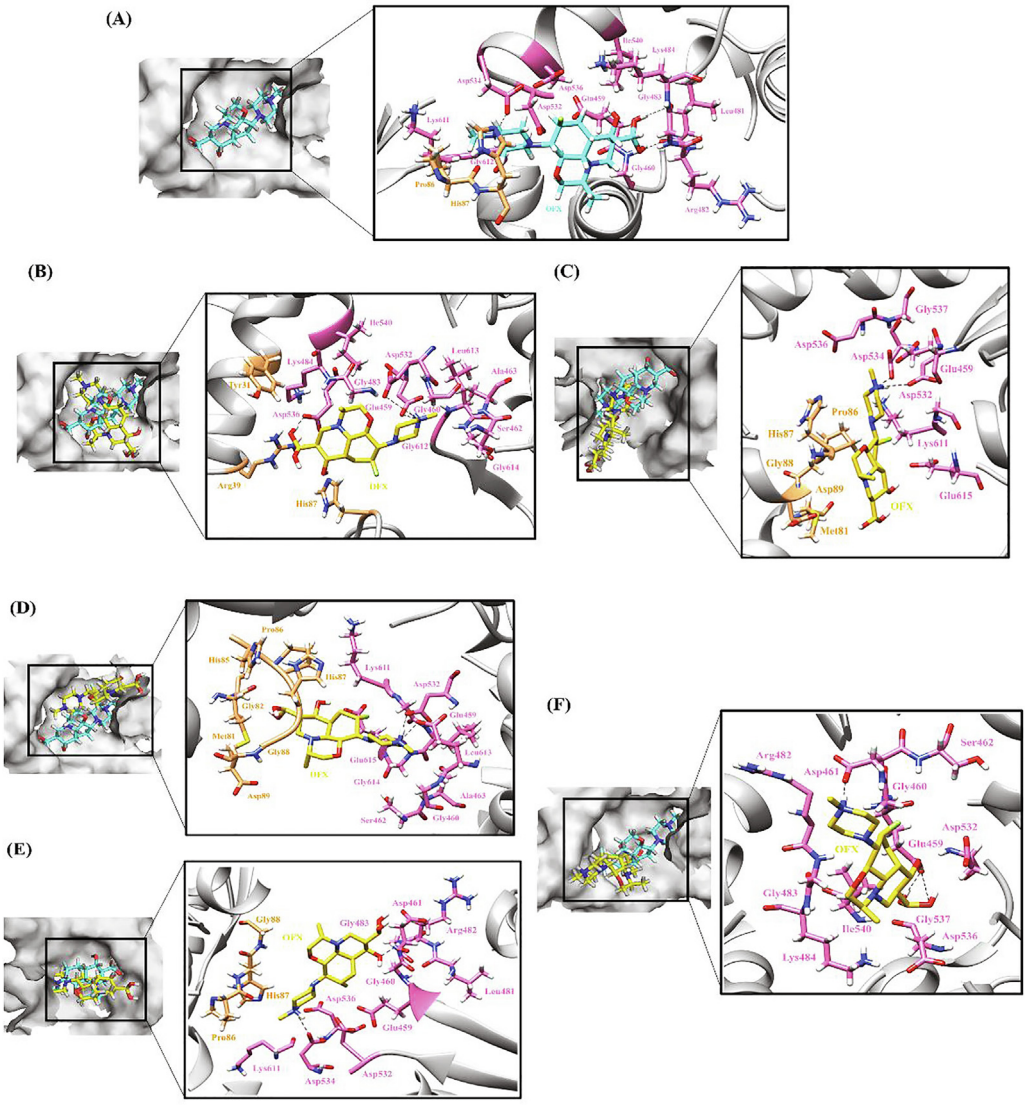

Fig. 9. Hydrogen bonding and hydrophobic interactions in DNA gyrase-OFX complex. (A) WT (B) L96P (C) D472A (D) R392C (E) R495H (F) R446C. The left panel is a view of the drug inside the binding pocket of protein and the right panel illustrates protein residues interacting with the drug. OFX is shown in cyan in WT and yellow in mutants. Hydrogen bonding and hydrophobic residues are shown in orange for GyrA-NTD and pink for GyrB-CTD. Black dashed lines represent hydrogen bonds. (For interpretation of the references to colour in this figure legend, the reader is referred to the web version of this article.)

Substitution of Asp with His as in the case of D8H mutant structure resulted in the formation of more intense inter-atomic interactions (hydrophobic and hydrogen) with the surrounding residues and altered environment of the binding pocket. The sustained rigidity depicts lower flexibility in D8H mutant with ENCOM values for $\Delta\Delta S_{Vib}$ reaching down to −0.16. Upon ligand binding, D8H mutation did not interfere much with the hydrophobic structure of the binding pocket and thus all polar interactions and the H-bonds with PZA were retained as found in WT. An increase in docking score can be due to the rotation of the aromatic ring of PZA which caused the ligand to come in close proximity to Trp68 which besides the pi-pi interaction enhanced the hydrophobicity of the pocket, thus enabling Trp68 to firmly stack with nearby hydrophobic residues. In WT, change from Cys138 to Arg enriched the hydrophobic environment of the binding pocket. Moreover, the tendency of Arg to form salt-bridges with Asp placed the Asp49 in the vicinity of PZA, helps in the restoration of key H-bond with its carbonyl oxygen group enabling the mutant C138R to maintain an efficient docking score of −4.7. The stable and compact binding can also be substantiated by the surge in interatomic interactions in the mutant which explains the lower flexibility value, $\Delta\Delta S_{Vib}$ ENCOM of −0.465.

Mutations W119G/L presented comparable results by keeping intact most of the interactions visible in WT. In W119G, a change in the position of Asp8 and Phe13 caused a gentle constriction in the binding site thus bringing down the docking score to −4.5 only. On the other hand, a shift of docking score to −4.4 was seen in W119L caused by stacking of interacting hydrophobic residues and loss of the critical H-bond at Cys138 eventually disorienting the drug within the binding site (Fig. 8B). Besides the difference in the stability of the static conformations of W119G/L, the complex of both mutations did not form the multitudes of interactions as the flexibility values were recorded to be 1.442 and 0.889 in W119G and W119L, respectively. Mutations A46E/P/V display variations of docking capacities among each other at the single codon position. Although, due to the rise in hydrophobic interactions and H-bonds within the complex, all the three mutants replicated the results of WT in displaying reduced complex flexibilities with the $\Delta\Delta S_{Vib}$ ENCOM values of −0.254, −0.185 and −0.249 in A46E, A46P and A46V, respectively.

Compared to the WT, A46P showed the minute shift in docking score, −4.6, due to its presence near the loop forming residues (51–77) that comprise the mouth of the binding site [43]. On the other hand, the docking scores of A46E (-4.4) and A46V (-4.4) were lower than the WT due to fewer hydrophobic residues in these two mutants and also because of the absence of pi-pi interaction at Trp68 compared to the WT. Fig. 8C and 8D illustrate H-bonding and hydrophobic interactions between PZA and A46E and A46V mutant proteins, respectively.

The docking scores in V128A and V128G were close to that of WT and found to be −4.7 and −4.6, respectively. The increased entropies associated with Ala and Gly induced flexibility in the protein with $\Delta\Delta S_{Vib}$ ENCOM values being 0.537 and 0.992 each for V128A and V128G. In V128A, the altered positions of hydrophobic Phe13 and Leu19 residues turned out to be favorable for the drug and enhanced its binding with PncA. However, the change in positions of residues, Asp8 and Phe13, in case of V128G resulted in the constriction of the drug binding site but a polar interaction by the nearby His57 slightly restored the binding stability resulting in a very little change from the WT.

The docking score in L120P is −4.4 which shows ineffective binding compared to the WT. The mutation resulted in the loss of crucial Ile133 H-bond and pi-pi interaction with Trp68 and an increase in hydrophobic residues causing deformity in the binding site and thus ligand disorientation. The impact of fewer H-bonds is also reflected from the increased flexibility value of 0.342 in case L120P. The docking score of L116P was recorded to be −4.6 which signals the unaffected interaction of a mutant in comparison to WT except a slight positional movement in Phe13 and Leu19. Being hydrophobic, they tend to remain shifted towards the hydrophobic clusters which causes the slight constriction within the binding site. Moreover, the reduced interatomic interactions soared the flexibility score to 1.041.

DNA gyrase: The docking scores (in kcal/mol) for WT were found to be −7.3, −6.8, −8.2 and −4.8 for OFX, MFX, CIF and LFX, respectively. As compared to WT, ΔG was reduced in A90V (-5.0, −4.8, −4.0, −3.7), S91P (-4.6, −3.3, −4.0, −2.9), D94A (-6.0, −4.8, −3.9, −3.8), D94G (-4.3, −4.9, −4.6, −3.5) and D94N (-3.3, −4.3, −6.6, −3.5) of GyrA and D461N (-3.6, −2.8, −4.3, −4.3), D461H (-4.9, −3.7, −4.3, −4.1), N499D (-2.8, −5.4, −6.1, −4.0) and E501V (-2.9, −3.4, −4.9, −3.2) of GyrB, exhibiting the reduced binding affinity of drugs (in the order OFX, MFX and CIF) in these mutants. In DNA gyrase, for benign mutation S95T the docking scores for OFX, MFX, CIF and LFX were −6.4, −6.4, −7.2 and −3.5, respectively which were lower in comparison to WT.

Fluoroquinolones were docked in the binding pocket of WT and mutant DNA gyrase which is composed of GyrA-NTD (codons 2–500) and GyrB-CTD (codons 426–675) [44]. The strong interaction between the WT DNA gyrase and the ligands are attributed to the formation of 3 (OFX), 3 (MFX), 2 (CIF) and 3 (LFX) H-bonds, salt bridges and hydrophobic interactions and alterations in these interactions was seen in case of mutants leading to disrupted drug binding (Fig. 9A). The impact of DNA gyrase mutations, A90V, S91P, D94G/A/N, D461N/H, N499D and E501V on drug binding has already been reported [84,85,114–116]. Large scale effect of mutations was observed in case of binding of OFX in contrast to CIF and MOX as OFX behaves as H-bond acceptor more than CIF and MFX [117].

The QRDR L96P mutation led to a declined score compared to the WT (Fig. 9B) since Proline is a non-favored substitution residue known to introduce kink in the structure and thus disrupting the protein structure and inducing disorientation of ligand as evident from our analysis of the mutation L96P [57].

R309Q showed a drastic reduction in binding affinity for OFX and CIF as compared to WT. CIF forms a H-bond with Glu459 moving towards GyrA-NTD which leads to breakage of H-bonds with Gly614. Substitution of Arg to Gln induced a significant reduction in hydrophobic interacting residues and made the ligand exposed to the solvent further making it inaccessible to the binding pocket. Negligible changes were observed in the case of MFX and LFX.

As already mentioned in the case of RpoB, substitution from His is not favorable, the same was observed in H368Q mutation [57]. The weak interatomic interactions in the mutant lead to an increase in the flexibility ($\Delta\Delta S_{Vib}$ ENCOM 0.358) of the native protein. Further, ligand disorientation in the binding pocket and alterations in H-bonds as well as decreased hydrophobicity were noticed. H368Q mutation had maximum impact on binding of OFX followed by CIF, MFX and least by LFX.

In QRDR mutation D472A, change from Asp to a Ala, a comparatively less bulky AA is reported to be a disfavored substitution [103]. This led to the loss of interactions between the ligand and active residues Asp532, Asp534 and Asp536 of protein, which did not let the ligand reach the binding pocket (Fig. 9C).

In R392C, the substitution of polar and positively charged AA by a non-polar, neutral and low molecular weight residue led to the reduced binding affinity of the drugs as evident from their docking scores, which can also correspond to their high MIC value on DST [84]. Substitution of Arg by Cys resulted in the loss of side chain interaction with the surrounding residues leading to the slight increase in protein flexibility ($\Delta\Delta S_{Vib}$ ENCOM 0.186). CIF in complex with mutant protein completely overlapped with CIF-WT complex, a slight reduction in hydrophobicity was found accompanied by increase in H-bonds. Similar was the observation in MFX-R392C complex where MFX shifted slightly more towards GyrA-NTD. However, a major difference was seen in case of OFX and LFX. OFX could not enter the binding pocket and moved towards GyrA-NTD where it settled in a horizontal conformation on the surface (Fig. 9D). The orientation of LFX changed from horizontal in WT to vertical in case of mutant.

Although His is generally considered favorable at active sites and thus induces rigidity and stability, the mutant R495H resulted in decreased molecular flexibility. This may be due to the loss of side chain interactions made by the WT Arg with the neighboring residues. In the mutant protein complexed with OFX (Fig. 9E) and MFX, the drugs could not reach the binding pocket as much as in case of WT. CIF and LFX drifted from the binding pocket and moved away from GyrB and largely towards GyrA.

In secondary mutations, the decrease in docking scores in R446C (-4.3, −4.7, −5.8, −3.3 kcal/mol), T511N (-4.2, −4.7, −4.6, −3.5 kcal/mol) and G512R (-2.1, −2.2, −4.8, −3.5 kcal/mol) depicts altered binding of the drugs within the binding site and needs in-depth evaluation. Similar to R392C, Arg substitution to Cys at position 446 increased the overall flexibility of the molecule ($\Delta\Delta S_{Vib}$ ENCOM 0.697), and reduced the overall binding affinity of OFX, MFX, CIF and LFX due to a weaker hydrophobic network and a smaller number of H-bonds. Fig. 9F portrays the positioning of OFX in the binding pocket of DNA gyrase where the drug, in case of mutant R446C, did not reach the binding pocket in its entirety and moved away from GyrA-NTD.

In the T511N mutation, Asn introduced flexibility ($\Delta\Delta S_{Vib}$ ENCOM 0.309) in the molecule. The low docking score with drugs is evidence of the failure of the ligand to interact with the Asp532 and Asp536 catalytic residues, driving the ligand disorientation.

In the case of G512R, mutation from non-polar to polar AA resulted in an increase in the interacting residues making the mutant protein more rigid ($\Delta\Delta S_{Vib}$ ENCOM −0.746). But in the G512R-drug complex, the drugs, MFX and CIF, were unable to reach the depth of the binding pocket as compared to WT due to the loss in all the H-bonds. A huge influence of this mutation was seen in the case of OFX and LFX where OFX placed itself entirely on the surface of GyrB and LFX totally drifted away from the binding pocket.

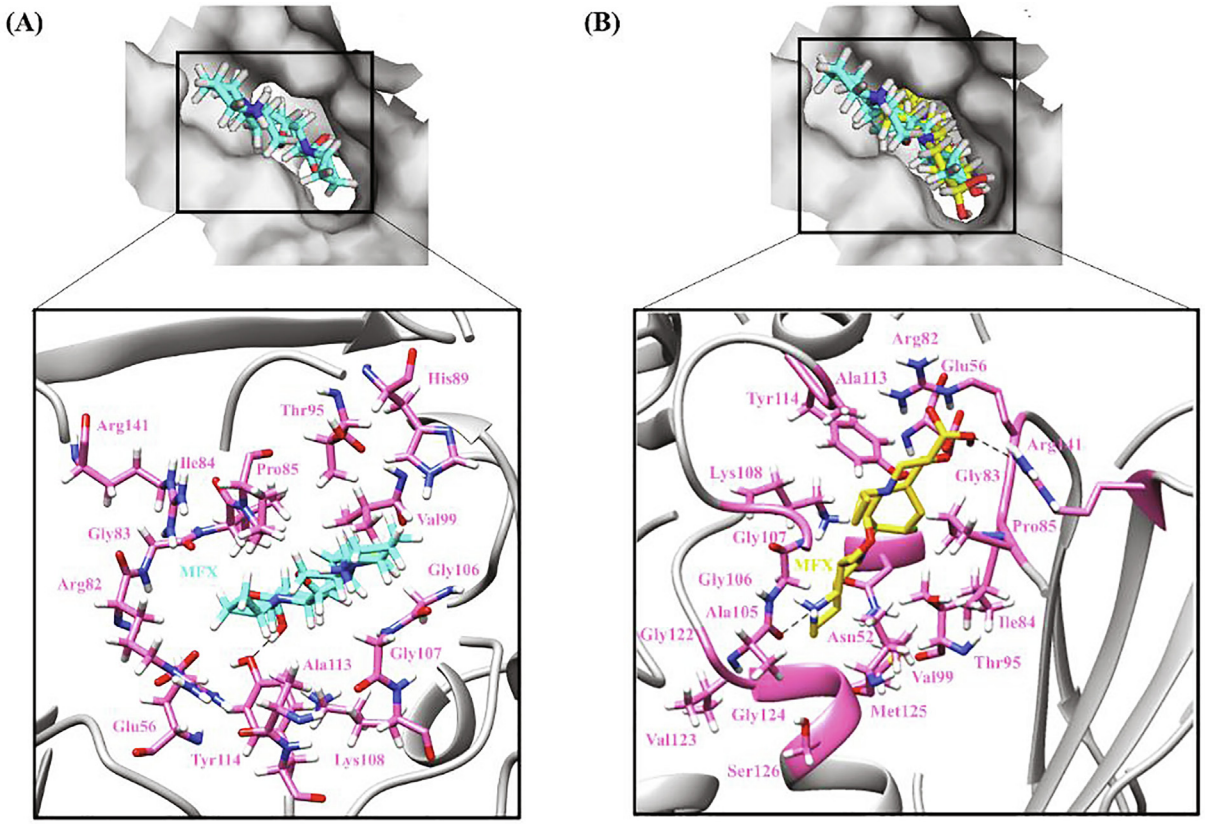

Fig. 10. Hydrogen bonding and hydrophobic interactions in DNA gyrase (ATPase)-MFX complex. (A) WT (B) V125M. The top panel is a view of the drug inside the binding pocket of protein and the right panel illustrates protein residues interacting with the drug. MFX is shown in cyan in WT and yellow in mutants. Hydrogen bonding and hydrophobic residues are shown in pink. Black dashed lines represent hydrogen bonds. (For interpretation of the references to colour in this figure legend, the reader is referred to the web version of this article.)

With the emergence of DR-isolates with varied genetic composition, enumerating the importance of less focused GyrA-CTD and GyrB-NTD has become equally pivotal. GyrA-CTD is involved in binding and wrapping the DNA [118] but the mutations found in this domain had very lesser effects on the stability, functionality and pathogenicity of the protein by our analyses and thus, were not considered for protein–ligand docking studies. GyrB-NTD harbors the ATPase activity and is known to have binding sites for other drugs like coumarins. Mutations in this domain along with GyrA-NTD and GyrB-CTD have been found to be involved in drug resistance in clinical isolates [118]. Thus, highly destabilizing and deleterious mutations from this domain were analyzed further for their effect on drug binding affinity.

V125M which is an active residue of GyrB-NTD resulted in increased molecular rigidity ($\Delta\Delta S_{Vib}$ ENCOM −0.499) as a result of the construction of a multibranched network of bonds with the nearby residues. The mutant protein showed similar affinity for OFX (-5.5) and LFX (-3.6), reduced affinity for MFX (-2.7) and increased for CIF (-7.6) as compared to WT OFX (-5.5), LFX (-3.7), MFX (-5.7) and CIF (-5.0). V125 is part of the ATP lid region and is disordered in nature [119] due to which its substitution by Met induced large conformational changes in binding of drugs. The enhanced stability of the V125M-CIF complex is due to the more hydrophobic environment in case of mutant than WT. With OFX, the mutation led to loss of H-bonds but also increasing the number of hydrophobic residues around the ligand and thus exhibiting similar affinity as WT. LFX completely overlapped in case of WT and mutant and a slightly reduced binding affinity was due to loss of hydrophobic residues in mutant protein–ligand complex. In the V125-MFX complex, the ligand rotated and moved inwards towards Sulphur moiety of Met resulting in formation of new hydrogen bonds where in WT protein, the ligand was entirely surrounded by hydrophobic network forming residues (Fig. 10A and 10B).

In mutant R212S, Arg interacts with the surrounding residues using hydrogen, ionic and weak interactions, thus replacement of this residue with a neutral and less bulky Ser enhances the flexibility of the molecule ($\Delta\Delta S_{Vib}$ ENCOM 0.773). Presence of Ser at 212 position led to the slight disorientation of the ligands and more exposure to the solvent thus forming new H-bonds. This was due to the presence of a OH group in its side chain which can form H-bonds with the protein backbone thus mimicking Pro [57].

Mutation R421H had binding affinity similar to WT. The mutant protein R421H was observed to have decreased flexibility ($\Delta\Delta S_{Vib}$ ENCOM −0.032) which might be due to the introduction of an aromatic ring by His. However, there was not much difference in the interactions with the neighboring residues in the mutant when compared to the WT protein.

3.7. Protein-protein interaction (PPI) analysis

Numerous PPI were obtained/computed for proteins coded by *rpoB*, *katG*, *inhA*, *pncA*, *gyrA* and *gyrB* genes by taking in account their reported co-expressions, fusions, gene neighborhood and co-occurrence. This was done to look into some crucial unexplored interactions which might affect the normal functioning of the proteins mentioned and subsequently impact the drug resistance.

RpoB: The PPI network of RpoB demonstrated, RpoA and RpoC proteins as its highly interacting and co-expressing partners with the confidence score >=0.9. Mutations in RpoA and RpoC are

already known for their significant role in RIF drug resistance owing to which various studies are now exploring the role of RpoA and RpoC as compensatory targets against *M.tb* [120]. Other interacting partners of RpoB included RpsL, RpsK, RpsC, RpsL, RpsG, RpsH and RpsE known for conferring resistance to streptomycin. Moreover, RpsL generates dysfunctional ribosome due to mutations [121], affecting transcription and translation efficiencies ultimately leading to disruption of the machinery, therefore challenging the transcription-translation coupling [122] while the role of remaining interacting partners is not yet studied. Indeed, observations [123] in clinical populations of bacterial pathogens suggest the existence of undiscovered interactions [124]. Thus, there is an urgent need to uncover the spectrum of mutations that suppress the costs arising from epistatic interactions in multidrug-resistant pathogens.

InhA: The highly interacting partners of InhA as analyzed by the STRING PPI network were found to be FabH, KasA, and FabG. Biosynthesis of mycolic acids involves two distinct pathways FAS-I and FAS-II. The InhA, KasA, and FabG work together in the FAS-II system where FabH serves as a connecting link between the two systems determining its relative importance in the mycolic acid synthesis. The involvement of co-expressing InhA and FabG genes in drug resistance is well established [61]. The mutations present in their regulatory region are known to confer INH and ethionamide (ETH) resistance however, the involvement of FabG coding region in ethionamide resistance is not known. Moreover, the higher expression of essential KasA and its compensatory mutations are known to be present in clinical isolates in response to INH stress. Targeting this particular overexpressed protein in INH resistant isolates where InhA is partially or completely deactivated due to mutations, would further deprive the bacteria of its necessary mycolic acid production pathway. The subsequent deactivation of both the essential InhA and KasA proteins would obstruct bacterial replication and survival [125].

KatG: The results of KatG PPI network demonstrated FurA and Rv1907c proteins as its highly interacting and co-expressing partners with the confidence score >=0.9. KatG and FurA are well-studied proteins and mutations in them are known to be highly associated with INH drug resistance. Conversely, their third co-expression partner Rv1907c, already reported for its suspected role in INH resistance by *in silico* studies [126], is still an uncharacterized conserved hypothetical protein. Other interacting partners of katG included superoxide dismutase (SodA and SodC) and alkylhydroperoxidase (AhpC) proteins which are involved in superoxide degeneration pathway and are known to partially compensate for the loss of KatG protein activity in INH-resistant strains. AhpC protects the pathogen against hydrogen peroxides and its hyper-expression due to the presence of compensatory mutations has also been linked to various INH-resistant strains [127]. Therefore, it would be interesting to elucidate the action of interaction partners like Rv1907c and AhpC which might reveal more players contributing to INH resistance. Further studies on their possible function inside the pathogen and involvement in acquiring drug resistance could project Rv1907c and AhpC as novel therapeutic targets to counter INH-resistant *M.tb*.

PncA: String analysis of PncA reported interactions with an uncharacterized protein Rv2044c that scores high for the fusion and co-expression. PncA is known to be present downstream of Rv2044c. A frameshift deletion in Rv2044c has been reported that eliminates its stop codon causing its protein to fuse with the downstream PncA. It results in the complex formation of PncA and Rv2044c with a novel and uncharacterized domain DUF2784 [128]. Such a phenomenon is bound to alter the existing pattern of functionality in PncA. It would be interesting to note the consequences of this event in PncA keeping in mind its association with the drug resistance. The newly explored functions and role of such uncharacterized domains could elucidate the alternative pathways that could be exploited to halt the *M.tb* pathogenesis.

Another high confidence scoring (co-expression, co-occurrence and vicinity) interacting partner for PncA was bifunctional NAD(P)H-hydrate repair enzyme (nnr). PncA is known to have a role in deamination of nicotinamide into nicotinate, required for the salvage pathway of nucleotide biosynthesis. Meanwhile the protein NNR (NAD(P)H-hydrate) is required for the epimerization of the NAD(P)HX, a damaged form of NAD(P)H, thus providing a crucial metabolic factor required for basic cellular function and biosynthetic pathways. The interaction between PncA and NNR within the genome demands an in-depth analysis of their conjoint role keeping in focus their possible contribution in conferring resistance against the drug PZA [129].

DNA gyrase: Interestingly, all the drug resistance associated proteins included in this study (RpoB, KatG, InhA, and PncA) were found to be high confidence interacting partners of GyrA and GyrB. Any mutations leading to malfunction in these proteins would directly affect the properties of cells and other interacting partners by changing their expression profiles. Further subsequent mutations in interacting proteins [130,131] may also be responsible for the conversion of mono fluoroquinolone resistant isolates to MDR or XDR. Recombinant proteins, RecA and RecF, the high confidence DNA gyrase interacting proteins are involved in the SOS pathway which is known to be upregulated in *M.tb* persister cells [132]. Targeting these proteins in recalcitrant bacterial subpopulation can be advantageous in improving the efficacy as well as shortening the anti-TB regimen. Another interacting protein is DNA topoisomerase I (TopA) which is emerging as an attractive anti-mycobacterial drug target against which chemotherapeutic agents are being developed to inhibit transcription in persisters [133].

3.8. MycoTRAP-DB database

Our MycoTRAP-DB is an online database that harbors almost all the mutations present in six putative first- and second-line drug resistance associated genes (*rpoB, inhA, katG, pncA, gyrA* and *gyrB*). Other than just assembling the mutations, it also provides information about implications of these mutations on the structures and functions of proteins coded by these genes. The database can be used for searching, retrieving, analyzing and downloading the data of mutations present in drug resistant *M.tb* clinical isolates. MycoTRAP-DB presents information about mutations which have been studied for diagnosis of drug resistance in TB, however, there are other mutations identified to be pathogenic by various sequence and structure-based tools used in the present study. Future experimental studies can focus on these pathogenic mutations to decipher their possible roles and accountability for causing drug resistance and develop more efficient genotypic methods for diagnosis and detection of drug resistant TB. The database is accessible at http://139.59.12.92.

4. Conclusion

An increase in the number of MDR and XDR-TB cases has aggravated the problem of TB worldwide, urging the need to improvise treatment strategies against DR-TB. The breakneck advances in the genomics and computational biology have led to the upgradation in the genomic and transcriptomic data. With the evolution of the microorganisms, mutations have been incorporated into their genomes which may provide them with the evolutionary and ecological advantages. Extensive data for these mutations are available in various widely known databases, but the lack of the updated database places a vacuum among the investigators

approaching the real-time reported data. An in-house database, MycoTRAP-DB, of almost all the reported mutations (till December 2020) in resistant and sensitive strains of *M.tb* was prepared for the genes *rpoB, inhA, katG, pncA, gyrA* and *gyrB*. This database brings most of the dispersed information about drug susceptible or resistant polymorphisms at a single place and would also open up the gateway to utilize this dataset to derive a convincing solution against DR-TB. The study is focused on non-synonymous mutations in specific genes encoding drug targets and any variations, primarily non-synonymous being able to alter protein structure, in these genes could affect the function of protein as well as its affinity for the drug resulting in drug resistance. Moreover, from our comprehensive dataset, we identified several secondary mutations which had a similar impact on protein structure and function as compared to known prevalent mutations in target genes: a finding that prompted us to look into the impact of these mutations on the pathogenesis of TB.

Molecular docking studies conducted to explore the impact of mutations on drug-binding revealed a correlation between the docking scores and reported MIC values for WT and mutant protein-drug complexes. The mutations which were found to have scored lower than their respective WT proteins have also been known to have higher MIC. This reflects a relationship between the structural stability of the complex with the reported MIC values. The RpoB mutations, S456W, D441C, H451C, H451Q, H451T and H451R scored contrastingly lower than WT and these results are also supported by the reported higher MIC values [96]. In case of InhA, the I21T and I21V mutants are found to be associated with promoter region mutation mostly with C-15 T. The MIC for only C-15 T was recorded as 8 μg/ml but with co-occurrence of I21T it increased to 32 μg/ml [134]. The MIC for another low scoring mutation, S94A of InhA was 8 μg/ml [134] against WT 0.2 μg/mL [135]. The lesser docking scores for KatG mutations R128G, T275P, W300G and W321G, as compared to WT, correlate with their known resistance profiles and MIC values derived from INH-DST (1–10 μg/ml) [111,136]. PncA also followed the similar trend as higher MIC value has been reported for its lowest scoring mutation A46P [137]. The drastic reduction in docking scores of mutations reportedly having higher MIC values was also found in case of GyrA and GyrB against OFX, MFX, LFX and CIF. The low scoring mutations, A90V, S91P, D94A, D94G and D94N of GyrA and D461N, D461H, N499D and E501V of GyrB have been stated to have higher MIC values on DST 0.25 to 2 μg/ml (OFX), 0.06 to 0.5 μg/ml (MFX), LFX 0.12–1 μg/ml and 1–8 mg/L (CIF) [138]. The comparison of MIC of these drugs for the WT *M.tb* $H_{37}Rv$ ($\leq$0.5 mg/L for OFX, $\leq$0.125 mg/L for MFX and $\leq$ 1 mg/L for CIF) [125]. Furthermore, high MIC values have been shown for mutation R392C [84] and the secondary mutations, R446C, T511N and G512R of DNA gyrase [84,85,89].

The systematic approach used in this study has the ability to expand our understanding related to the mechanism of resistance associated with a particular mutation. However, the results presented in this study are mere predictions and form the foreground for further experimental validations to establish the impact of the identified mutations. The information can be exploited in future by investigating the resistance profile of the *M.tb* strain from the clinical sample prior to the drug administration process. The most prevalent and evolutionary important mutations can be used for the advancement of drug designing. Drug repurposing can be done to make use of the FDA approved drugs which may bind to the mutant phenotype of the protein with better binding affinity. Also, combination therapy may be incorporated into the drug designing where the combination of the drugs which inhibits two or more common mutant phenotypes of the protein can be developed.

5. Data Availability

The database, MycoTRAP-DB is publicly accessible at http://139.59.12.92. All the other data are available as supplementary data.

CRediT authorship contribution statement

Pooja Singh: Investigation, Data curation, Writing - original draft. **Salma Jamal:** Methodology, Investigation, Writing - original draft. **Faraz Ahmed:** Investigation, Writing - original draft. **Najumu Saqib:** Investigation. **Seema Mehra:** Investigation, Writing - original draft. **Waseem Ali:** Investigation, Writing - original draft. **Deodutta Roy:** . **Nasreen Z. Ehtesham:** Conceptualization, Writing - original draft. **Seyed E. Hasnain:** Conceptualization, Funding acquisition.

Declaration of Competing Interest

The authors declare that they have no known competing financial interests or personal relationships that could have appeared to influence the work reported in this paper.

Acknowledgements

S.J. and S.M. acknowledge a Young Scientist Fellowship from the Department of Health Research (DHR), India. S.E.H. is a J.C. Bose National Fellow, Department of Science and Technology, Government of India and Robert Koch Fellow, Robert Koch Institute, Berlin, Germany.

Funding

S.E.H. was supported by North East Grants (BT/PR23099/NER/95/632/2017), (BT/PR23155/NER/95/634/2017) from Department of Biotechnology (DBT), Ministry of Science and Technology, Government of India.

Appendix A. Supplementary data

Supplementary data to this article can be found online at https://doi.org/10.1016/j.csbj.2021.04.034.

References

[1] Crubézy E, Legal L, Fabas G, Dabernat H, Ludes B. Pathogeny of archaic mycobacteria at the emergence of urban life in Egypt (3400 BC). Infect Genet Evol 2006;6(1):13–21.
[2] Organization WH (2020) Global tuberculosis report 2020: executive summary.
[3] Chakaya JM, Marais B, du Cros P, Ntoumi F, Mfinanga S, Kapata N, et al. Programmatic versus personalised approaches to managing the global epidemic of multidrug-resistant tuberculosis. Lancet Respir Med 2020;8(4):334–5.
[4] Rahman SA, Singh Y, Kohli S, Ahmad J, Ehtesham NZ, Tyagi AK, Hasnain SE. Comparative analyses of nonpathogenic, opportunistic, and totally pathogenic mycobacteria reveal genomic and biochemical variabilities and highlight the survival attributes of Mycobacterium tuberculosis. mBio 2014;5.
[5] Ahmed N, Dobrindt U, Hacker J, Hasnain SE. Genomic fluidity and pathogenic bacteria: applications in diagnostics, epidemiology and intervention. Nat Rev Microbiol 2008;6(5):387–94.
[6] Ventola CL. The antibiotic resistance crisis: part 1: causes and threats. P T 2015;40:277–83.
[7] Parsa K, Hasnain SE. Proteomics of multidrug resistant Mycobacterium tuberculosis clinical isolates: a peep show on mechanism of drug resistance & perhaps more. Indian J Med Res 2015;141:8–9.
[8] Eldholm V, Balloux F. Antimicrobial resistance in Mycobacterium tuberculosis: The odd one out. Trends Microbiol 2016;24(8):637–48.

[9] Siddiqi N, Pathak N, Banerjee S, Ahmed N, Katoch VM, Hasnain SE, et al. Mycobacterium tuberculosis isolate with a distinct genomic identity overexpresses a tap-like efflux pump. Infection 2004;32(2):109–11.
[10] Comas I, Borrell S, Roetzer A, Rose G, Malla B, Kato-Maeda M, et al. Whole-genome sequencing of rifampicin-resistant Mycobacterium tuberculosis strains identifies compensatory mutations in RNA polymerase genes. Nat Genet 2012;44(1):106–10.
[11] Ragland DA, Nalivaika EA, Nalam MNL, Prachanronarong KL, Cao H, Bandaranayake RM, et al. Drug resistance conferred by mutations outside the active site through alterations in the dynamic and structural ensemble of HIV-1 protease. J Am Chem Soc 2014;136(34):11956–63.
[12] Karen van Niekerk RP, Reva ON, Korostetskiy IS, Ilin AI, Akhmetova GK. Basic Biology and Applications of Actinobacteria, 2018. 1 - Shymaa Enany Y1–2018-12-05 ed.
[13] Hasnain SE, O'Toole RF, Grover S, Ehtesham NZ. Whole genome sequencing: a new paradigm in the surveillance and control of human tuberculosis. Tuberculosis (Edinb) 2015;95(2):91–4.
[14] Miotto P, Tessema B, Tagliani E, Chindelevitch L, Starks AM, et al. A standardised method for interpreting the association between mutations and phenotypic drug resistance in Mycobacterium tuberculosis. Eur Respir J 2017;50.
[15] Majeed AA, Ahmed N, Rao KR, Ghousunnissa S, Kauser F, et al. AmpliBASE MT: a Mycobacterium tuberculosis diversity knowledgebase. Bioinformatics 2004;20:989–92.
[16] Chernyaeva EN, Shulgina MV, Rotkevich MS, Dobrynin PV, Simonov SA, Shitikov EA, et al. Genome-wide Mycobacterium tuberculosis variation (GMTV) database: a new tool for integrating sequence variations and epidemiology. BMC Genomics 2014;15(1):308. https://doi.org/10.1186/1471-2164-15-308.
[17] Sandgren A, Strong M, Muthukrishnan P, Weiner BK, Church GM, Murray MB. Tuberculosis drug resistance mutation database. PLoS Med 2009;6:e2.
[18] Flandrois JP, Lina G, Dumitrescu O. MUBII-TB-DB: a database of mutations associated with antibiotic resistance in Mycobacterium tuberculosis. BMC Bioinf 2014;15:107.
[19] Jamal S, Khubaib M, Gangwar R, Grover S, Grover A, Hasnain SE. Author Correction: Artificial Intelligence and Machine learning based prediction of resistant and susceptible mutations in Mycobacterium tuberculosis. Sci Rep 2020;10:14660.
[20] Pires DE, Chen J, Blundell TL, Ascher DB. In silico functional dissection of saturation mutagenesis: Interpreting the relationship between phenotypes and changes in protein stability, interactions and activity. Sci Rep 2016;6:19848.
[21] Hameed HMA, Islam MM, Chhotaray C, Wang C, Liu Y, Tan Y, et al. Molecular Targets Related Drug Resistance Mechanisms in MDR-, XDR-, and TDR-Mycobacterium tuberculosis Strains. Front Cell Infect Microbiol 2018;8. https://doi.org/10.3389/fcimb.2018.00114.
[22] Zhang Lu, Zhao Y, Gao Y, Wu L, Gao R, Zhang Qi, et al. Structures of cell wall arabinosyltransferases with the anti-tuberculosis drug ethambutol. Science 2020;368(6496):1211–9.
[23] Iacobino A, Fattorini L, Giannoni F. Drug-Resistant Tuberculosis 2020. Where We Stand. 2020;10(6):2153. https://doi.org/10.3390/app10062153.
[24] Rodrigues CH, Pires DE, Ascher DB. DynaMut: predicting the impact of mutations on protein conformation, flexibility and stability. Nucleic Acids Res 2018;46:W350–5.
[25] Consortium CR, the GP, Allix-Beguec C, Arandjelovic I, Bi L et al. (2018) Prediction of Susceptibility to First-Line Tuberculosis Drugs by DNA Sequencing. N Engl J Med 379: 1403-1415.
[26] Bendl J, Stourac J, Salanda O, Pavelka A, Wieben ED, Zendulka J, Brezovsky J and Damborsky J (2014) PredictSNP: robust and accurate consensus classifier for prediction of disease-related mutations. PLoS Comput Biol 10: e1003440.
[27] Mi H, Dong Q, Muruganujan A, Gaudet P, Lewis S and Thomas PD (2010) PANTHER version 7: improved phylogenetic trees, orthologs and collaboration with the Gene Ontology Consortium. Nucleic Acids Res 38: D204-210.
[28] Capriotti E, Calabrese R, Casadio R. Predicting the insurgence of human genetic diseases associated to single point protein mutations with support vector machines and evolutionary information. Bioinformatics 2006;22(22):2729–34.
[29] Ramensky V, Bork P, Sunyaev S. Human non-synonymous SNPs: server and survey. Nucleic Acids Res 2002;30:3894–900.
[30] Adzhubei IA, Schmidt S, Peshkin L, Ramensky VE, Gerasimova A, Bork P, et al. A method and server for predicting damaging missense mutations. Nat Methods 2010;7(4):248–9.
[31] Ng PC, Henikoff S. SIFT: Predicting amino acid changes that affect protein function. Nucleic Acids Res 2003;31:3812–4.
[32] Bromberg Y, Rost B. SNAP: predict effect of non-synonymous polymorphisms on function. Nucleic Acids Res 2007;35(11):3823–35.
[33] Worth CL, Preissner R, Blundell TL. SDM–a server for predicting effects of mutations on protein stability and malfunction. Nucleic Acids Res 2011;39:W215–22.
[34] Quan L, Lv Q, Zhang Y. STRUM: structure-based prediction of protein stability changes upon single-point mutation. Bioinformatics 2016;32(19):2936–46.
[35] Pires DE, Ascher DB and Blundell TL (2014) mCSM: predicting the effects of mutations in proteins using graph-based signatures. Bioinformatics 30: 335-342.
[36] Pires DE, Blundell TL, Ascher DB. mCSM-lig: quantifying the effects of mutations on protein-small molecule affinity in genetic disease and emergence of drug resistance. Sci Rep 2016;6:29575.
[37] Schrodinger. (2011). LLC, New York.
[38] Berman HM, Westbrook J, Feng Z, Gilliland G, Bhat TN, Weissig H, et al. The Protein Data Bank. Nucleic Acids Res 2000;28:235–42.
[39] Lin W, Mandal S, Degen D, Liu Yu, Ebright YW, Li S, et al. Structural Basis of Mycobacterium tuberculosis Transcription and Transcription Inhibition. Mol Cell 2017;66(2):169–179.e8.
[40] Dessen A, Quemard A, Blanchard J, Jacobs W, Sacchettini J. Crystal structure and function of the isoniazid target of Mycobacterium tuberculosis. Science 1995;267(5204):1638–41.
[41] Bertrand T, Eady NAJ, Jones JN, Jesmin, Nagy JM, Jamart-Grégoire B, et al. Crystal structure of Mycobacterium tuberculosis catalase-peroxidase. J Biol Chem 2004;279(37):38991–9.
[42] Munir A, Wilson MT, Hardwick SW, Chirgadze DY, Worrall JAR, Blundell TL, et al. Using cryo-EM to understand antimycobacterial resistance in the catalase-peroxidase (KatG) from Mycobacterium tuberculosis. Structure 2021. https://doi.org/10.1016/j.str.2020.12.008.
[43] Petrella S, Gelus-Ziental N, Maudry A, Laurans C, Boudjelloul R, Sougakoff W, et al. Crystal structure of the pyrazinamidase of Mycobacterium tuberculosis: insights into natural and acquired resistance to pyrazinamide. PLoS ONE 2011;6(1):e15785.
[44] Blower TR, Williamson BH, Kerns RJ, Berger JM. Crystal structure and stability of gyrase-fluoroquinolone cleaved complexes from Mycobacterium tuberculosis. Proc Natl Acad Sci U S A 2016;113(7):1706–13.
[45] Oliveira JS, Pereira JH, Canduri F, Rodrigues NC, de Souza ON, de Azevedo WF, et al. Crystallographic and pre-steady-state kinetics studies on binding of NADH to wild-type and isoniazid-resistant enoyl-ACP(CoA) reductase enzymes from Mycobacterium tuberculosis. J Mol Biol 2006;359(3):646–66.
[46] Vilcheze C, Wang F, Arai M, Hazbon MH, Colangeli R, Kremer L, et al. Transfer of a point mutation in Mycobacterium tuberculosis inhA resolves the target of isoniazid. Nat Med 2006;12:1027–9.
[47] Madhavi Sastry G, Adzhigirey M, Day T, Annabhimoju R, Sherman W. Protein and ligand preparation: parameters, protocols, and influence on virtual screening enrichments. J Comput Aided Mol Des 2013;27(3):221–34.
[48] Arbex MA, Varella Mde C, Siqueira HR, Mello FA. Antituberculosis drugs: drug interactions, adverse effects, and use in special situations. Part 1: first-line drugs. J Bras Pneumol 2010;36:626–40.
[49] Kim S, Thiessen PA, Bolton EE, Chen J, Fu G, Gindulyte A, et al. PubChem Substance and Compound databases. Nucleic Acids Res 2016;44(D1):D1202–13.
[50] Metcalfe C, Macdonald IK, Murphy EJ, Brown KA, Raven EL, Moody PCE. The tuberculosis prodrug isoniazid bound to activating peroxidases. J Biol Chem 2008;283(10):6193–200.
[51] Piton J, Petrella S, Delarue M, André-Leroux G, Jarlier V, Aubry A, et al. Structural insights into the quinolone resistance mechanism of Mycobacterium tuberculosis DNA gyrase. PLoS ONE 2010;5(8):e12245.
[52] Friesner RA, Banks JL, Murphy RB, Halgren TA, Klicic JJ, et al. Glide: a new approach for rapid, accurate docking and scoring. 1. Method and assessment of docking accuracy. J Med Chem 2004;47:1739–49.
[53] Frappier V, Najmanovich RJ, MacKerell AD. A coarse-grained elastic network atom contact model and its use in the simulation of protein dynamics and the prediction of the effect of mutations. PLoS Comput Biol 2014;10(4):e1003569.
[54] UniProt C. The universal protein resource (UniProt). Nucleic Acids Res 2008;36:D190–5.
[55] Altschul SF, Madden TL, Schaffer AA, Zhang J, Zhang Z, Miller W, et al. Gapped BLAST and PSI-BLAST: a new generation of protein database search programs. Nucleic Acids Res 1997;25:3389–402.
[56] Szklarczyk D, Gable AL, Lyon D, Junge A, Wyder S et al. (2019) STRING v11: protein-protein association networks with increased coverage, supporting functional discovery in genome-wide experimental datasets. Nucleic Acids Res 47: D607-D613.
[57] Rudnicki WR, Mroczek T, Cudek P. Amino acid properties conserved in molecular evolution. PLoS ONE 2014;9:e98983.
[58] Rouse DA, Li Z, Bai GH, Morris SL. Characterization of the katG and inhA genes of isoniazid-resistant clinical isolates of Mycobacterium tuberculosis. Antimicrob Agents Chemother 1995;39(11):2472–7.
[59] Sheen P, Ferrer P, Gilman RH, López-Llano J, Fuentes P, Valencia E, et al. Effect of pyrazinamidase activity on pyrazinamide resistance in Mycobacterium tuberculosis. Tuberculosis (Edinb) 2009;89(2):109–13.
[60] Siddiqi N, Shamim M, Hussain S, Choudhary RK, Ahmed N, Prachee, et al. Molecular characterization of multidrug-resistant isolates of Mycobacterium tuberculosis from patients in North India. Antimicrob Agents Chemother 2002;46(2):443–50.
[61] Vilcheze C and Jacobs WR, Jr. (2014) Resistance to Isoniazid and Ethionamide in Mycobacterium tuberculosis: Genes, Mutations, and Causalities. Microbiol Spectr 2: MGM2-0014-2013.
[62] Portelli S, Phelan JE, Ascher DB, Clark TG, Furnham N. Understanding molecular consequences of putative drug resistant mutations in Mycobacterium tuberculosis. Sci Rep 2018;8:15356.
[63] Maruri F, Sterling TR, Kaiga AW, Blackman A, van der Heijden YF, Mayer C, Cambau E and Aubry A (2012) A systematic review of gyrase mutations associated with fluoroquinolone-resistant Mycobacterium tuberculosis and a proposed gyrase numbering system. J Antimicrob Chemother 67: 819-831.

[64] Brossier F, Veziris N, Aubry A, Jarlier V, Sougakoff W. Detection by GenoType MTBDRsl test of complex mechanisms of resistance to second-line drugs and ethambutol in multidrug-resistant Mycobacterium tuberculosis complex isolates. J Clin Microbiol 2010;48(5):1683–9.
[65] Park H, Bradley P, Greisen P, Liu Y, Mulligan VK, Kim DE, et al. Simultaneous optimization of biomolecular energy functions on features from small molecules and macromolecules. J Chem Theory Comput 2016;12 (12):6201–12.
[66] Kellogg EH, Leaver-Fay A, Baker D. Role of conformational sampling in computing mutation-induced changes in protein structure and stability. Proteins 2011;79(3):830–8.
[67] Merker M, Kohl TA, Barilar I, Andres S, Fowler PW, Chryssanthou E, et al. Phylogenetically informative mutations in genes implicated in antibiotic resistance in Mycobacterium tuberculosis complex. Genome Med 2020;12(1). https://doi.org/10.1186/s13073-020-00726-5.
[68] Singhal R, Reynolds PR, Marola JL, Epperson LE, Arora J, Sarin R, et al. Sequence analysis of fluoroquinolone resistance-associated genes gyrA and gyrB in clinical mycobacterium tuberculosis isolates from patients suspected of having multidrug-resistant tuberculosis in New Delhi, India. J Clin Microbiol 2016;54(9):2298–305.
[69] Yamaguchi T, Yokoyama K, Nakajima C and Suzuki Y (2017) Quinolone resistance-associated amino acid substitutions affect enzymatic activity of Mycobacterium leprae DNA gyrase. Biosci Biotechnol Biochem 81: 1343-1347.
[70] Rifat D, Campodónico VL, Tao J, Miller JA, Alp A, Yao Y, et al. In vitro and in vivo fitness costs associated with Mycobacterium tuberculosis RpoB mutation H526D. Future Microbiol 2017;12(9):753–65.
[71] Brandis G, Hughes D. Genetic characterization of compensatory evolution in strains carrying rpoB Ser531Leu, the rifampicin resistance mutation most frequently found in clinical isolates. J Antimicrob Chemother 2013;68 (11):2493–7.
[72] Casali N, Nikolayevskyy V, Balabanova Y, Ignatyeva O, Kontsevaya I, Harris SR, et al. Microevolution of extensively drug-resistant tuberculosis in Russia. Genome Res 2012;22(4):735–45.
[73] Walker TM, Kohl TA, Omar SV, Hedge J, Del Ojo Elias C, Bradley P, et al. Whole-genome sequencing for prediction of Mycobacterium tuberculosis drug susceptibility and resistance: a retrospective cohort study. Lancet Infect Dis 2015;15(10):1193–202.
[74] Chen X, He G, Wang S, Lin S, Chen J, Zhang W. Evaluation of whole-genome sequence method to diagnose resistance of 13 anti-tuberculosis drugs and characterize resistance genes in clinical multi-drug resistance Mycobacterium tuberculosis isolates from China. Front Microbiol 2019;10:1741.
[75] Gagneux S, Burgos MV, DeRiemer K, Enciso A, Muñoz S, Hopewell PC, et al. Impact of bacterial genetics on the transmission of isoniazid-resistant Mycobacterium tuberculosis. PLoS Pathog 2006;2:e61.
[76] Pym AS, Saint-Joanis B, Cole ST. Effect of katG mutations on the virulence of Mycobacterium tuberculosis and the implication for transmission in humans. Infect Immun 2002;70(9):4955–60.
[77] van Soolingen D, de Haas PW, van Doorn HR, Kuijper Ed, Rinder H, Borgdorff M. Mutations at amino acid position 315 of the katG gene are associated with high-level resistance to isoniazid, other drug resistance, and successful transmission of Mycobacterium tuberculosis in the Netherlands. J Infect Dis 2000;182(6):1788–90.
[78] Sheen P, Lozano K, Gilman RH, Valencia HJ, Loli S, Fuentes P, et al. pncA gene expression and prediction factors on pyrazinamide resistance in Mycobacterium tuberculosis. Tuberculosis (Edinb) 2013;93(5):515–22.
[79] Aung HL, Tun T, Moradigaravand D, Köser CU, Nyunt WW, Aung ST, et al. Whole-genome sequencing of multidrug-resistant Mycobacterium tuberculosis isolates from Myanmar. J Glob Antimicrob Resist 2016;6:113–7.
[80] Cuevas-Córdoba B, Xochihua-González SO, Cuellar A, Fuentes-Domínguez J, Zenteno-Cuevas R. Characterization of pncA gene mutations in pyrazinamide-resistant Mycobacterium tuberculosis isolates from Mexico. Infect Genet Evol 2013;19:330–4.
[81] Chiu YC, Huang SF, Yu KW, Lee YC, Feng JY, Su WJ. Characteristics of pncA mutations in multidrug-resistant tuberculosis in Taiwan. BMC Infect Dis 2011;11:240.
[82] Allana S, Shashkina E, Mathema B, Bablishvili N, Tukvadze N, Shah NS, et al. pncA Gene mutations associated with pyrazinamide resistance in drug-resistant tuberculosis, South Africa and Georgia. Emerg Infect Dis 2017;23 (3):491–5.
[83] Shi J, Su R, Zheng D, Zhu Y, Ma X, Wang S, et al. Pyrazinamide resistance and mutation patterns among multidrug-resistant Mycobacterium tuberculosis from Henan Province. Infect Drug Resist 2020;13:2929–41.
[84] Farhat MR, Jacobson KR, Franke MF, Kaur D, Sloutsky A, Mitnick CD, et al. Gyrase Mutations are associated with variable levels of fluoroquinolone resistance in Mycobacterium tuberculosis. J Clin Microbiol 2016;54 (3):727–33.
[85] Malik S, Willby M, Sikes D, Tsodikov OV, Posey JE, Via LE. New insights into fluoroquinolone resistance in Mycobacterium tuberculosis: functional genetic analysis of gyrA and gyrB mutations. PLoS ONE 2012;7(6):e39754.
[86] Salah Eldin A, Mostafa NM, Mostafa SI. Detection of fluoroquinolone resistance in Mycobacterium tuberculosis clinical isolates as determined by gyrA/B gene mutation by using PCR technique. Egypt J Chest Dis Tubercul 2012;61(4):349–53.
[87] Pantel A, Petrella S, Veziris N, Brossier F, Bastian S, Jarlier V, et al. Extending the definition of the GyrB quinolone resistance-determining region in Mycobacterium tuberculosis DNA gyrase for assessing fluoroquinolone resistance in M. tuberculosis. Antimicrob Agents Chemother 2012;56 (4):1990–6.
[88] Yin X, Yu Z. Mutation characterization of gyrA and gyrB genes in levofloxacin-resistant Mycobacterium tuberculosis clinical isolates from Guangdong Province in China. J Infect 2010;61(2):150–4.
[89] Chien J-Y, Chiu W-Y, Chien S-T, Chiang C-J, Yu C-J, Hsueh P-R. Mutations in gyrA and gyrB among fluoroquinolone- and multidrug-resistant Mycobacterium tuberculosis isolates. Antimicrob Agents Chemother 2016;60(4):2090–6.
[90] Hameed HMA, Tan Y, Islam MM, Guo L, Chhotaray C, Wang S, et al. Phenotypic and genotypic characterization of levofloxacin- and moxifloxacin-resistant Mycobacterium tuberculosis clinical isolates in southern China. J Thorac Dis 2019;11(11):4613–25.
[91] Miotto P, Zhang Y, Cirillo DM, Yam WC. Drug resistance mechanisms and drug susceptibility testing for tuberculosis. Respirology 2018;23(12):1098–113.
[92] Yi L, Aono A, Chikamatsu K, Igarashi Y, Yamada H, Takaki A and Mitarai S (2017) In vitro activity of sitafloxacin against Mycobacterium tuberculosis with gyrA/B mutations isolated in Japan. J Med Microbiol 66: 770-776.
[93] Kabir S, Tahir Z, Mukhtar N, Sohail M, Saqalein M, Rehman A. Fluoroquinolone resistance and mutational profile of gyrA in pulmonary MDR tuberculosis patients. BMC Pulm Med 2020;20:138.
[94] Disratthakit A, Prammananan T, Tribuddharat C, Thaipisuttikul I, Doi N, Leechawengwongs M, et al. Role of gyrB mutations in pre-extensively and extensively drug-resistant tuberculosis in thai clinical isolates. Antimicrob Agents Chemother 2016;60(9):5189–97.
[95] Zhang Q, An X, Liu H, Wang S, Xiao T, Liu H. Uncovering the Resistance mechanism of Mycobacterium tuberculosis to rifampicin due to RNA Polymerase H451D/Y/R mutations from computational perspective. Front Chem 2019;7:819.
[96] Zaw MT, Emran NA, Lin Z. Mutations inside rifampicin-resistance determining region of rpoB gene associated with rifampicin-resistance in Mycobacterium tuberculosis. J Infect Public Health 2018;11(5):605–10.
[97] Hui J, Gordon N, Kajioka R. Permeability barrier to rifampin in mycobacteria. Antimicrob Agents Chemother 1977;11(5):773–9.
[98] Guerrero C, Stockman L, Marchesi F, Bodmer T, ROBERTS GD, Telenti A. Evaluation of the rpoB gene in rifampicin-susceptible and -resistant Mycobacterium avium and Mycobacterium intracellulare. J Antimicrob Chemother 1994;33(3):661–3.
[99] Figueiredo R, Ramos DF, Moiteiro C, Medeiros MA, Marcelo Curto MJ, Cardoso de Menezes J, et al. Pharmacophore insights into rpoB gene mutations in Mycobacterium tuberculosis rifampicin resistant isolates. Eur J Med Chem 2012;47:186–93.
[100] Williams DL, Spring L, Collins L, Miller LP, Heifets LB, Gangadharam PRJ, et al. Contribution of rpoB mutations to development of rifamycin cross-resistance in Mycobacterium tuberculosis. Antimicrob Agents Chemother 1998;42 (7):1853–7.
[101] Huitric E, Werngren J, Juréen P, Hoffner S. Resistance levels and rpoB gene mutations among in vitro-selected rifampin-resistant Mycobacterium tuberculosis mutants. Antimicrob Agents Chemother 2006;50(8):2860–2.
[102] Hwang HY, Chang CY, Chang LL, Chang SF, Chang YH, Chen YJ. Characterization of rifampicin-resistant Mycobacterium tuberculosis in Taiwan. J Med Microbiol 2003;52:239–45.
[103] Betts MJ and Russell RB. (2003), Bioinformatics for Geneticists, pp. 289-316.
[104] Telenti A, Imboden P, Marchesi F, Matter L, Schopfer K, Bodmer T, et al. Detection of rifampicin-resistance mutations in Mycobacterium tuberculosis. Lancet 1993;341(8846):647–51.
[105] Caws M, Duy PM, Tho DQ, Lan NTN, Hoa DV, Farrar J. Mutations prevalent among rifampin- and isoniazid-resistant Mycobacterium tuberculosis isolates from a hospital in Vietnam. J Clin Microbiol 2006;44(7):2333–7.
[106] Chikaonda T, Ketseoglou I, Nguluwe N, Krysiak R, Thengolose I, et al. Molecular characterisation of rifampicin-resistant Mycobacterium tuberculosis strains from Malawi. Afr J Lab Med 2017;6:463.
[107] Villar HO, Kauvar LM. Amino acid preferences at protein binding sites. FEBS Lett 1994;349:125–30.
[108] Ramaswamy S, Musser JM. Molecular genetic basis of antimicrobial agent resistance in Mycobacterium tuberculosis: 1998 update. Tuber Lung Dis 1998;79(1):3–29.
[109] Pimentel AL, de Lima Scodro RB, Caleffi-Ferracioli KR, Siqueira VLD, Campanerut-Sá PAZ, Lopes LDG, et al. Mutations in catalase-peroxidase KatG from isoniazid resistant Mycobacterium tuberculosis clinical isolates: insights from molecular dynamics simulations. J Mol Model 2017;23(4). https://doi.org/10.1007/s00894-017-3290-3.
[110] Marttila HJ, Soini H, Huovinen P, Viljanen MK. katG mutations in isoniazid-resistant Mycobacterium tuberculosis isolates recovered from Finnish patients. Antimicrob Agents Chemother 1996;40(9):2187–9.
[111] Jagielski T, Grzeszczuk M, Kaminski M, Roeske K, Napiorkowska A, Stachowiak R, et al. Identification and analysis of mutations in the katG gene in multidrug-resistant Mycobacterium tuberculosis clinical isolates. Pneumonol Alergol Pol 2013;81:298–307.
[112] Mo L, Zhang W, Wang J, Weng XH, Chen S, Shao LY, et al. Three-dimensional model and molecular mechanism of Mycobacterium tuberculosis catalase-peroxidase (KatG) and isoniazid-resistant KatG mutants. Microb Drug Resist 2004;10(4):269–79.

[113] Du X, Wang W, Kim R, Yakota H, Nguyen H, Kim S-H. Crystal structure and mechanism of catalysis of a pyrazinamidase from Pyrococcus horikoshii. Biochemistry 2001;40(47):14166–72.
[114] Pandey B, Grover S, Tyagi C, Goyal S, Jamal S, Singh A, et al. Dynamics of fluoroquinolones induced resistance in DNA gyrase of Mycobacterium tuberculosis. J Biomol Struct Dyn 2018;36(2):362–75.
[115] Chen J, Chen Z, Li Y, Xia W, Chen X, Chen T, et al. Characterization of gyrA and gyrB mutations and fluoroquinolone resistance in Mycobacterium tuberculosis clinical isolates from Hubei Province, China. Braz J Infect Dis 2012;16:136–41.
[116] Kim H, Nakajima C, Yokoyama K, Rahim Z, Kim YU, Oguri H, et al. Impact of the E540V amino acid substitution in GyrB of Mycobacterium tuberculosis on quinolone resistance. Antimicrob Agents Chemother 2011;55(8):3661–7.
[117] Daisy P, Vijayalakshmi P, Selvaraj C, Singh SK, Saipriya K. Targeting Multidrug Resistant Mycobacterium tuberculosis HtrA2 with Identical Chemical Entities of Fluoroquinolones. Indian J Pharm Sci 2012;74(3):217. https://doi.org/10.4103/0250-474X.106063.
[118] Huang YY, Deng JY, Gu J, Zhang ZP, Maxwell A, Bi LJ, Chen YY, Zhou YF, Yu ZN and Zhang XE (2006) The key DNA-binding residues in the C-terminal domain of Mycobacterium tuberculosis DNA gyrase A subunit (GyrA). Nucleic Acids Res 34: 5650-5659.
[119] Agrawal A, Roue M, Spitzfaden C, Petrella S, Aubry A, Hann M, Bax B and Mayer C (2013) Mycobacterium tuberculosis DNA gyrase ATPase domain structures suggest a dissociative mechanism that explains how ATP hydrolysis is coupled to domain motion. Biochem J 456: 263-273.
[120] Song T, Park Y, Shamputa IC, Seo S, Lee SY, et al. Fitness costs of rifampicin resistance in Mycobacterium tuberculosis are amplified under conditions of nutrient starvation and compensated by mutation in the beta' subunit of RNA polymerase. Mol Microbiol 2014;91:1106–19.
[121] Ruusala T, Andersson D, Ehrenberg M, Kurland CG. Hyper-accurate ribosomes inhibit growth. EMBO J 1984;3(11):2575–80.
[122] Ma C, Yang X, Lewis PJ. Bacterial Transcription as a Target for Antibacterial Drug Development. Microbiol Mol Biol Rev 2016;80(1):139–60.
[123] Arenz S, Wilson DN. Blast from the past: reassessing forgotten translation inhibitors, antibiotic selectivity, and resistance mechanisms to aid drug development. Mol Cell 2016;61(1):3–14.
[124] Casali N, Nikolayevskyy V, Balabanova Y, Harris SR, Ignatyeva O, Kontsevaya I, et al. Evolution and transmission of drug-resistant tuberculosis in a Russian population. Nat Genet 2014;46(3):279–86.
[125] Abrahams KA, Chung C-w, Ghidelli-Disse S, Rullas J, Rebollo-López MJ, Gurcha SS, et al. Identification of KasA as the cellular target of an anti-tubercular scaffold. Nat Commun 2016;7(1). https://doi.org/10.1038/ncomms12581.
[126] Beg MA, Shivangi, Thakur SC, Meena LS. Structural prediction and mutational analysis of Rv3906c gene of Mycobacterium tuberculosis H37Rv to determine its essentiality in survival. Adv Bioinformatics 2018;2018:1–12.
[127] Sherman DR, Mdluli K, Hickey MJ, Arain TM, Morris SL, Barry CE, et al. Compensatory ahpC gene expression in isoniazid-resistant Mycobacterium tuberculosis. Science 1996;272(5268):1641–3.
[128] Baddam R, Kumar N, Wieler LH, Lankapalli AK, Ahmed N, Peacock SJ, et al. Analysis of mutations in pncA reveals non-overlapping patterns among various lineages of Mycobacterium tuberculosis. Sci Rep 2018;8(1). https://doi.org/10.1038/s41598-018-22883-9.
[129] Marbaix AY, Noël G, Detroux AM, Vertommen D, Van Schaftingen E, Linster CL. Extremely conserved ATP- or ADP-dependent enzymatic system for nicotinamide nucleotide repair. J Biol Chem 2011;286(48):41246–52.
[130] Hu Y, Mangan JA, Dhillon J, Sole KM, Mitchison DA, Butcher PD, et al. Detection of mRNA transcripts and active transcription in persistent Mycobacterium tuberculosis induced by exposure to rifampin or pyrazinamide. J Bacteriol 2000;182(22):6358–65.
[131] Torrey HL, Keren I, Via LE, Lee JS, Lewis K, Kaufmann GF. High Persister Mutants in Mycobacterium tuberculosis. PLoS ONE 2016;11(5):e0155127.
[132] Choudhary E, Sharma R, Kumar Y, Agarwal N. Conditional Silencing by CRISPRi Reveals the Role of DNA Gyrase in Formation of Drug-Tolerant Persister Population in Mycobacterium tuberculosis. Front Cell Infect Microbiol 2019;9:70.
[133] Ravishankar S, Ambady A, Awasthy D, Mudugal NV, Menasinakai S, Jatheendranath S, et al. Genetic and chemical validation identifies Mycobacterium tuberculosis topoisomerase I as an attractive anti-tubercular target. Tuberculosis (Edinb) 2015;95(5):589–98.
[134] Morlock GP, Metchock B, Sikes D, Crawford JT, Cooksey RC. ethA, inhA, and katG loci of ethionamide-resistant clinical Mycobacterium tuberculosis isolates. Antimicrob Agents Chemother 2003;47(12):3799–805.
[135] Jhamb SS, Goyal A, Singh PP. Determination of the activity of standard anti-tuberculosis drugs against intramacrophage Mycobacterium tuberculosis, in vitro: MGIT 960 as a viable alternative for BACTEC 460. Braz J Infect Dis 2014;18(3):336–40.
[136] Heym B, Alzari PM, Honore N, Cole ST. Missense mutations in the catalase-peroxidase gene, katG, are associated with isoniazid resistance in Mycobacterium tuberculosis. Mol Microbiol 1995;15(2):235–45.
[137] Yadon AN, Maharaj K, Adamson JH, Lai Y-P, Sacchettini JC, Ioerger TR, et al. A comprehensive characterization of PncA polymorphisms that confer resistance to pyrazinamide. Nat Commun 2017;8(1). https://doi.org/10.1038/s41467-017-00721-2.
[138] Kaniga K, Cirillo DM, Hoffner S, Ismail NA, Kaur D, Lounis N, et al. A multilaboratory, multicountry study to determine MIC quality control ranges for phenotypic drug susceptibility testing of selected first-line antituberculosis drugs, second-line injectables, fluoroquinolones, clofazimine, and linezolid. J Clin Microbiol 2016;54(12):2963–8.